

NASA  
TP  
1898  
c. 1

NASA Technical Paper 1898

TECH LIBRARY KAFB, NM  
0134914

# Flight Test of a Pure-Tone Acoustic Source

Arnold W. Mueller and John S. Preisser

LOAN COPY; RETURN TO  
APWL TECHNICAL LIBRARY  
KIRTLAND AFB, N.M.

OCTOBER 1981



TECH LIBRARY KAFB, NM



0134914

NASA Technical Paper 1898

# Flight Test of a Pure-Tone Acoustic Source

Arnold W. Mueller and John S. Preisser  
*Langley Research Center*  
*Hampton, Virginia*

**NASA**

National Aeronautics  
and Space Administration

**Scientific and Technical  
Information Branch**

1981



CONTENTS

SUMMARY ..... 1

INTRODUCTION ..... 1

TEST DESCRIPTION ..... 2

    Acoustic Source ..... 2

    Outdoor Anechoic Test ..... 3

    Anechoic Flow Test ..... 4

    Flight Test ..... 5

        Test aircraft ..... 5

        Procedure ..... 7

        Tracking system ..... 8

        Acoustic system ..... 8

        Meteorological system ..... 9

DATA RESULTS AND DISCUSSION ..... 11

    Outdoor Anechoic Test ..... 11

    Anechoic Flow Test ..... 14

    Flight Test ..... 14

CONCLUDING REMARKS ..... 21

APPENDIX - FLIGHT-TO-STATIC DATA REDUCTION TECHNIQUE ..... 22

    Radar System ..... 22

    Acoustic System ..... 22

    Time Shifting ..... 22

    Ensemble Averaging ..... 24

    Weather System ..... 24

    Correction Procedure ..... 25

REFERENCES ..... 27

SYMBOLS ..... 28

## SUMMARY

A unique experiment involving static, flight, and open-jet testing of a pure-tone acoustic source has been conducted. The objectives of the experiment were (1) to determine if a 4-kHz tone radiated by a source and mixed with broadband aircraft flyover noise could be measured on the ground with a high degree of statistical confidence, (2) to determine how well a comparison could be made of a flight-to-static tone radiation pattern and a static radiation pattern, and (3) to determine if there were any installation effects on the radiation pattern due to the flight vehicle. Narrow-band acoustic data were measured with the aircraft flying over a speed range of 50 m/s to 80 m/s at a level altitude of 91 m. The data, ensemble averaged over an array of eight microphones, have a high statistical confidence and show excellent agreement when a comparison is made of the static to the flight-to-static radiation pattern. At shallow radiation angles, some undesirable effects of source installation were observed. Also discussed is the data reduction technique which was developed to merge the measured radar, weather, and acoustic data and to average and adjust the acoustic data for retarded time, spherical spreading, atmospheric absorption, ground impedance, instrumentation constraints, convective amplification, and Doppler shift.

## INTRODUCTION

Over the past decade, considerable effort has been made by many investigators to understand the effect of aircraft motion on noise generation and propagation. The basic aim has been to achieve a sufficient understanding of the so-called "flight effects" so that less expensive static tests could be employed to accurately predict the noise generated in flight. The major emphasis has been on studying jet exhaust noise and turbofan engine-inlet noise (e.g., refs. 1 and 2). Major differences have been found to exist between the static and flight noise fields. Unfortunately, for tests of these types, source alteration and propagation effects could not be sorted out, making any differences difficult to explain. To study a flight noise field in isolation, a simple noise source of known strength needed to be flight tested.

There are relatively few experimental studies in the literature involving simple noise sources in motion. Beran and Gething (ref. 3) used a sailplane with a speaker mounted in the wing to measure atmospheric attenuation effects. Norum and Liu (ref. 4) used a specially designed acoustic driver system to represent an acoustic monopole which was carried on top of an automobile. Their experiment was conducted over an asphalt surface. They found good agreement when comparing the static and forward-speed results using a complex normal impedance which represented a fairly hard acoustic surface. Recently, Hogstedt and Lowder (ref. 5) reported their work on measuring aircraft flyover noise propagation. Part of their work consisted of studying the feasibility of using an airborne reference noise source. One source, a siren, was mounted beneath a light airplane. A microphone was flush mounted in the siren throat to insure consistency of the acoustic source, and the far-field noise was measured by two ground-board systems. Results showed the usefulness of a constant repeatable noise source.

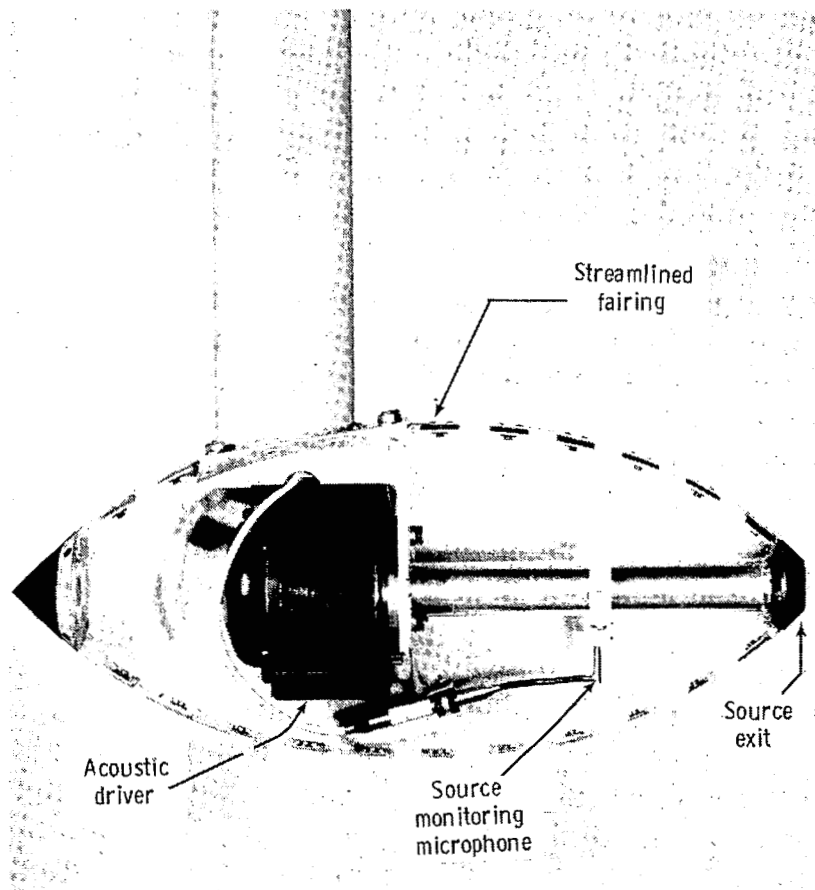
The present tests were conducted to study the propagation of a pure-tone source at a frequency (4 kHz) typical of inlet noise radiated by high-bypass-ratio turbofan engines. A simple acoustic source was tested in three environments, above an outdoor array of acoustic wedges, in an anechoic flow facility, and flown under the wing of a modified OV-1B aircraft. The OV-1B is the aircraft used in an ongoing NASA program to study flight effects of a turbofan engine.

The objectives of the present investigation were to determine if a flight noise-tone (4 kHz) radiation pattern could be measured on the ground with a high level of statistical confidence and to determine how well a comparison could be made between a flight-to-static radiation pattern and a static radiation pattern. A secondary objective was to ascertain if the noise field was adversely affected by the installation of the acoustic source on the aircraft. This latter effect could be significant if there were reflection or scattering of the radiated sound field by the aircraft.

#### TEST DESCRIPTION

##### Acoustic Source

A cutaway view of the pure-tone source is presented in figure 1. It consisted of a high-intensity acoustic driver coupled to a cylindrical tube and encased in an



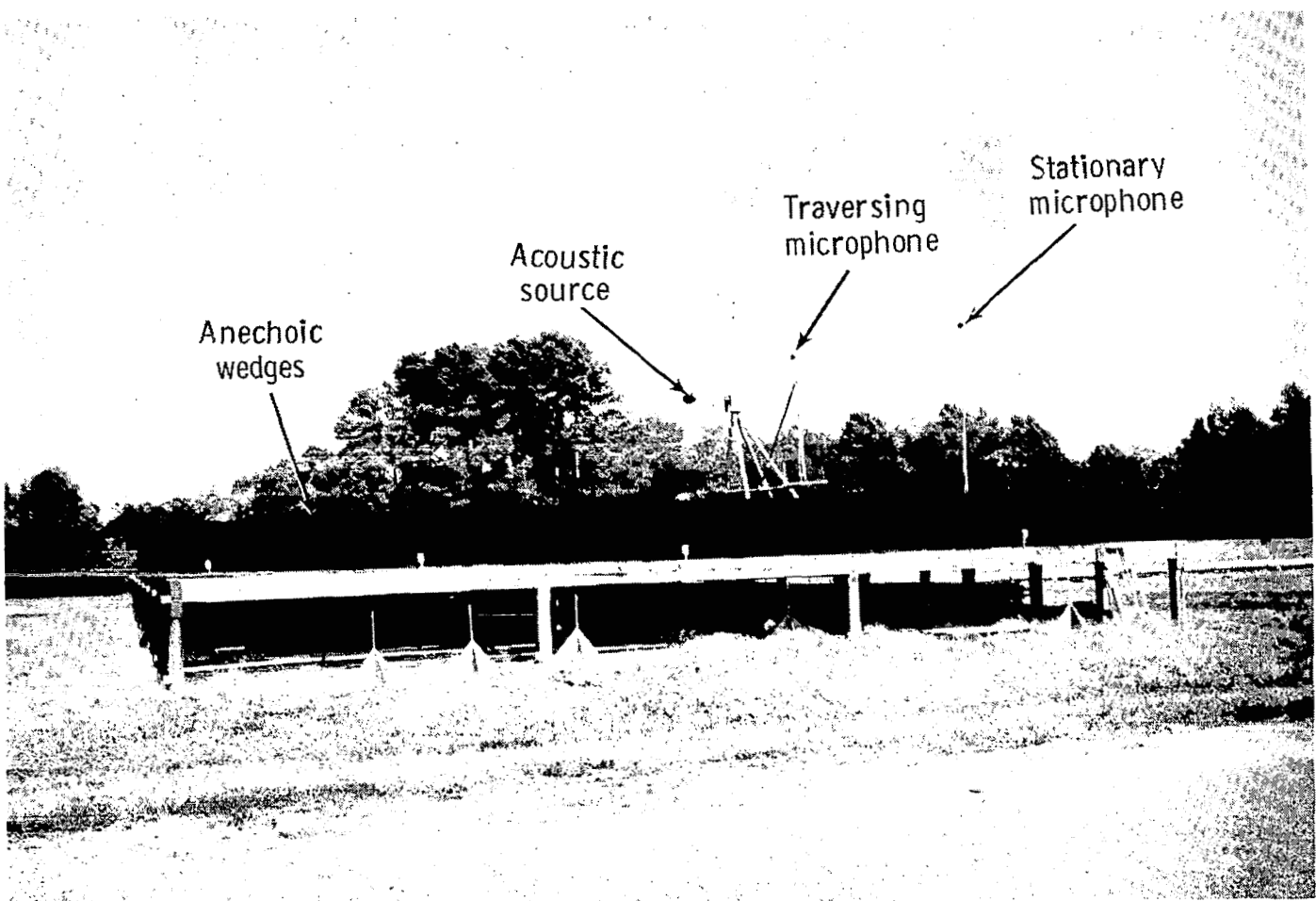
L-79-7363

Figure 1.- Cutaway view of pure-tone source.

aerodynamically streamlined fairing. The tube was 30.5 cm long and had a 3.5 cm inner diameter to match the size of the driver throat. This arrangement was designed to generate plane waves at the driver frequency of 4 kHz. A 0.32-cm microphone was flush mounted in the wall of the tube to monitor the source strength, and the end (source exit) was covered with a single layer of fiberglass cloth to inhibit unsteady aerodynamic fluctuations from affecting the acoustic source and to keep the driver and source microphone clean. The cloth is between 80 and 90 percent transmissive. Any change in the impedance at the cloth terminal location due to flow would show up as a change in the standing wave pattern inside the tube. The input voltage to the driver and the source microphone response was closely monitored at all times to insure constant source strength.

#### Outdoor Anechoic Test

Experiments were performed at the outdoor anechoic test apparatus at Langley Research Center in order to obtain the static radiation pattern at the selected source frequency. A photograph of the setup is presented in figure 2. The apparatus, located where background noise levels are low, contains a raised 12-m-square



L-79-7492

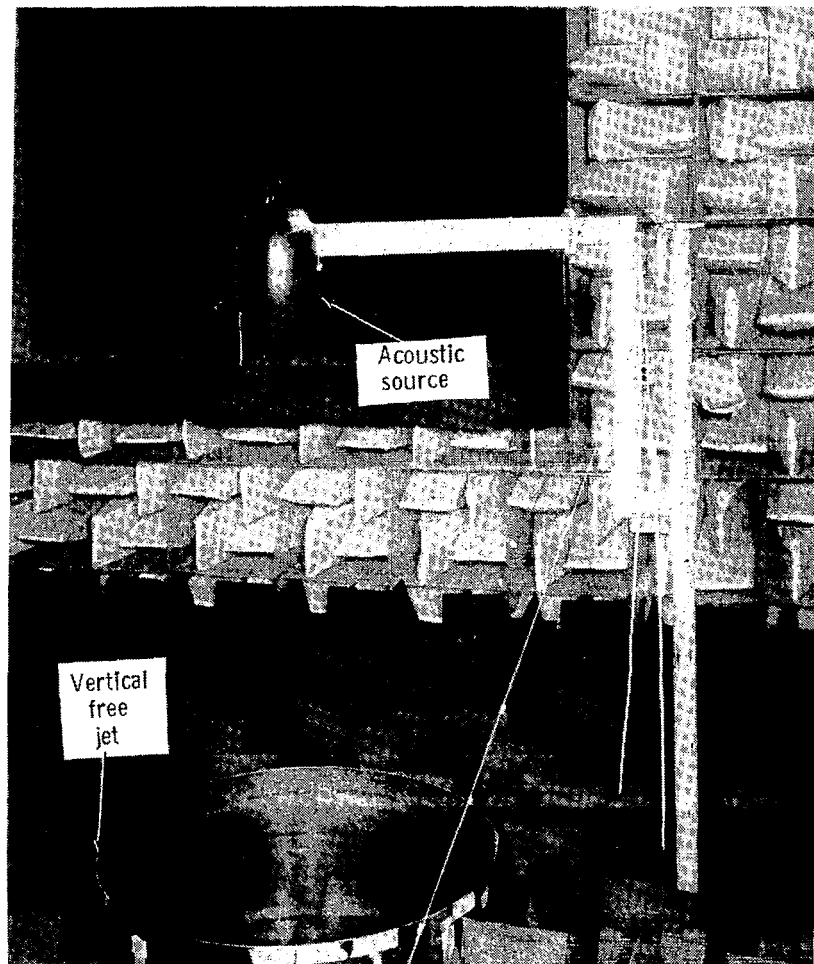
Figure 2.- Outdoor anechoic test area.

platform which is covered by anechoic wedges 0.84 m in height. The acoustic source, with its longitudinal axis parallel to the ground, was attached to a support structure 2.0 m above the wedges. A continuously traversing mechanism, at a radius of 4.6 m from the tube exit plane, rotated through  $110^{\circ}$  to measure the desired directivity patterns. A 1.27-cm condenser-type pressure microphone fitted with a grid cap and a windscreen was mounted atop the mechanism to measure the noise field. A similar microphone system was attached to a stationary pole and placed at a distance of 9.2 m from the source to insure that the traversing microphone was in the acoustic far field of the source.

Tests at a constant source frequency of 4 kHz were made for several source strengths. The data were high-pass filtered at 500 Hz and processed on-line to produce directivity patterns.

#### Anechoic Flow Test

The effect of simulated forward speed on the acoustic source was studied in the Langley Aircraft Noise Reduction Laboratory. Figure 3 presents a photograph of the source mounted at a height of 1.52 m above the exit plane of a 1.22-m-diameter



L-80-569

Figure 3.- Anechoic-flow-facility test.

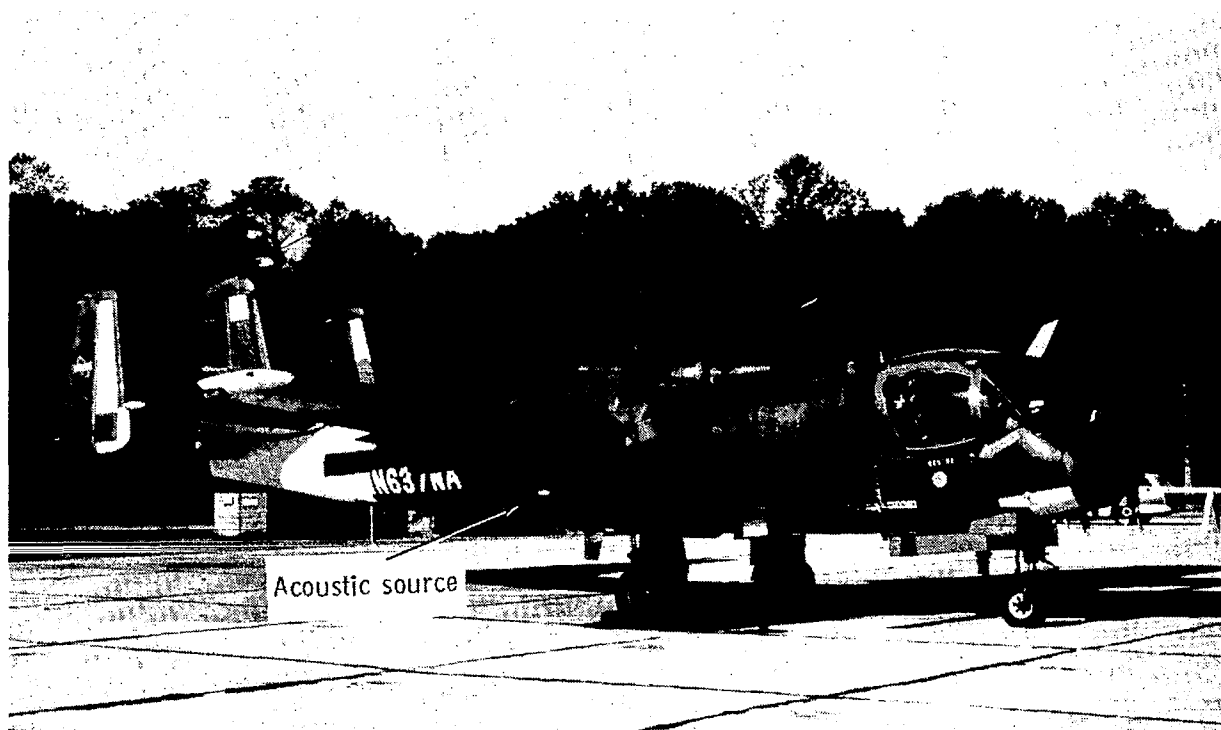


vertical jet in the anechoic chamber of the laboratory. The jet was run over a speed range of 0 to 35 m/s. The input voltage to the driver was kept constant over the speed range, and the internal source noise level was recorded to note any changes.

No radiation pattern data are presented however, due to the severe amplitude modulation of the pure tone (see ref. 6). The modulation, which is believed to be due to propagation of the signal through the jet's turbulent shear layer, resulted in direction scattering, spectral broadening, and a decrease in sound-pressure level thereby destroying the basic directivity of the source.

#### Flight Test

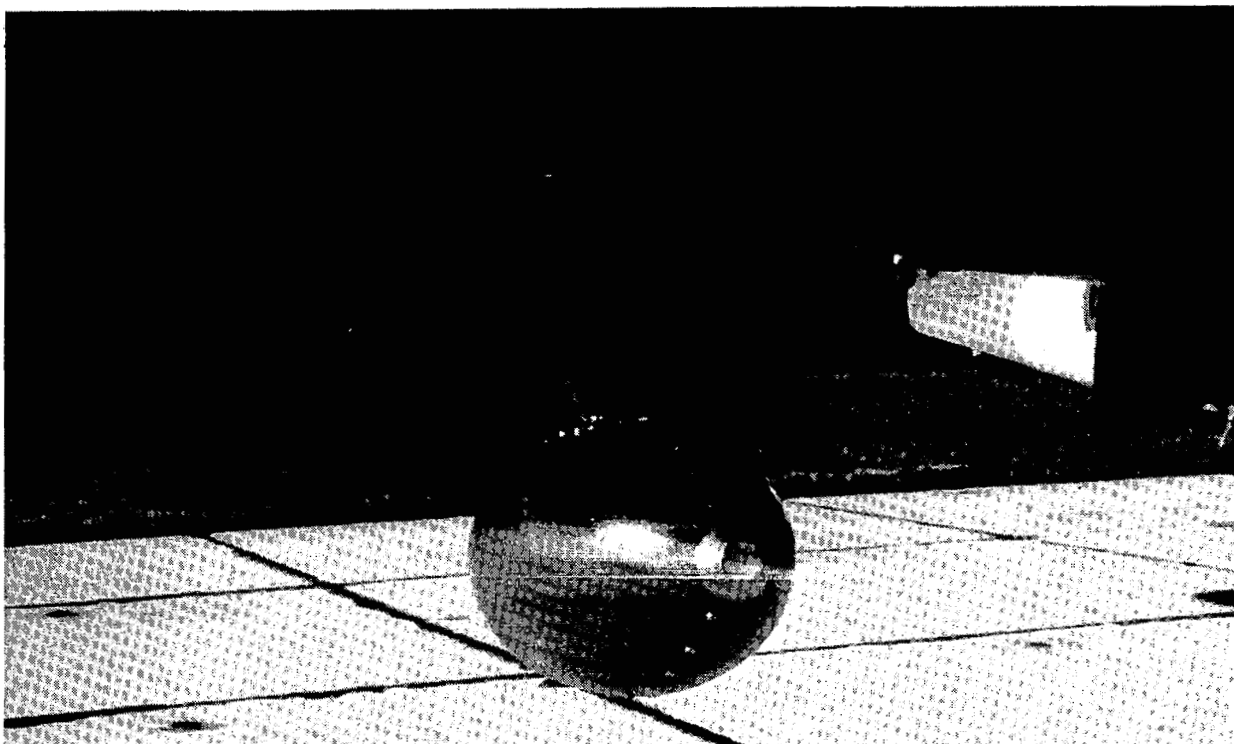
Test aircraft.- For the flight portion of the test program, conducted over a three-day period, the acoustic source was mounted underneath the starboard wing of the twin engine OV-1B aircraft. Photographs of the OV-1B with the source in place are shown in figure 4. The source was mounted on a pylon and attached to a bracket (fig. 4(b)) that normally holds an external fuel tank for the aircraft. In this position the source was 48 cm in back of (fig. 4(c)) and 64 cm to the side of the right engine propeller tip. Flight tests were conducted both with and without the right engine operating to determine if the rotating prop influenced the radiated noise field.



L-81-203

(a) Full view of OV-1B aircraft.

Figure 4.- Acoustic source mounted on OV-1B aircraft.



L-81-204

(b) Close-up frontal view of acoustic source.



L-81-205

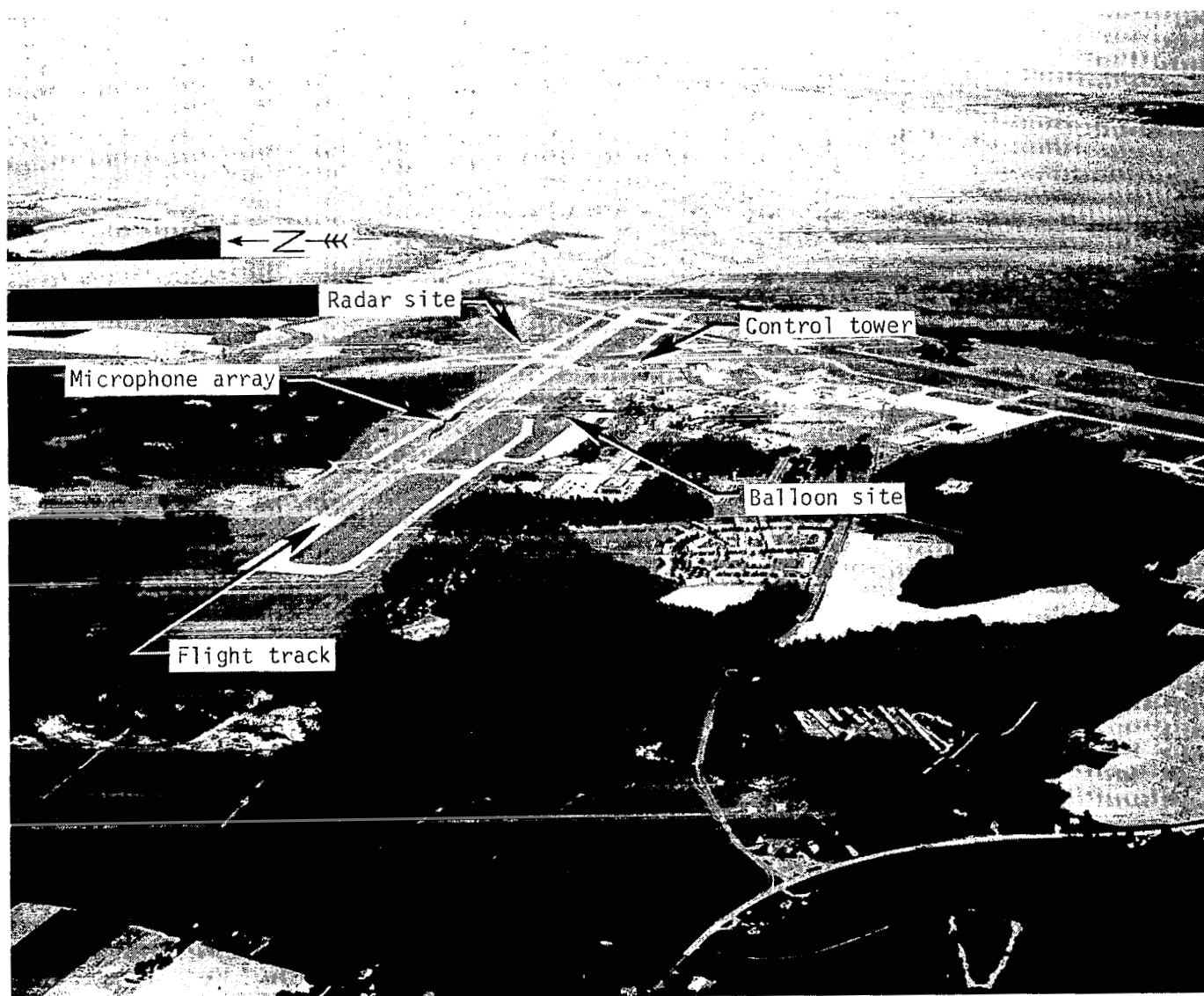
(c) Close-up side view of acoustic source.

Figure 4.- Concluded.

Test parameters included a constant source frequency of 4 kHz, a source amplitude of 140 dB in the horn, aircraft speeds between 50 m/s and 80 m/s, an aircraft altitude of approximately 91 m, and a constant power setting of the left OV-1B turboprop. Once the test parameters were selected for a given flyover, the pilot would use the rudder and ailerons to trim the aircraft so that the constant conditions could be maintained.

The frequency and amplitude of the voltage input to the driver and the horn response as monitored by the source microphone were recorded onboard using an FM tape recorder.

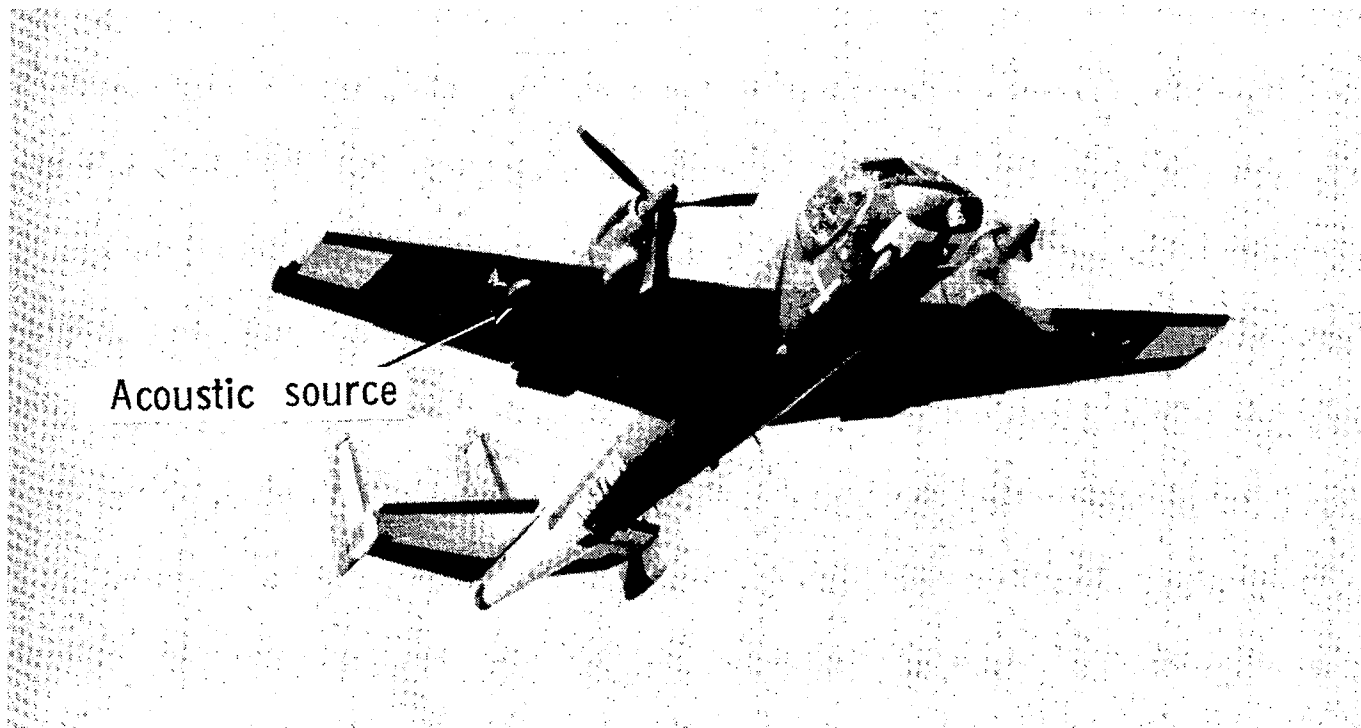
Procedure.- Figure 5 presents an aerial photograph of the test area at Wallops Flight Center. Typically, a flight consisted of multiple flyovers past an array of microphones located on the runway. The aircraft was tracked continuously by a laser



L-81-206

Figure 5.- Aerial photograph of test area at Wallops Flight Center.

radar. An onboard altimeter and airspeed indicator, as well as visual observation of the runway centerline, were used to obtain the desired test conditions. Real-time X-Y-Z aircraft positions and ground speeds (as well as a television view of the approaching aircraft) were displayed in the control tower. Figure 6 is a telephoto view showing the aircraft in flight over the microphone array with the right engine in a shutdown mode.



L-81-207

Figure 6.- Telephoto view of aircraft in flight with right turboprop shut down.

Tracking system.- The aircraft tracking system used to determine vehicle position consisted of a laser in conjunction with a FPS-16 radar. The system focused on a laser reflector located in a fairing directly under the nose of the aircraft (visible in fig. 4(a)). Tracking system accuracy is estimated to be  $\pm 0.15$  m in range and  $\pm 0.1$  mrad in angle. Each day the tracking system was calibrated with respect to the first microphone of the 9.1 m pole array.

Acoustic system.- As mentioned previously, microphones were placed on the runway to record the flyover noise. These were condenser-type pressure microphones (1.27 cm in diameter) fitted with grid caps and wind screens and positioned 4.6 m from the runway centerline. They were oriented such that as the airplane flew down the runway centerline, the source passed directly over the microphones which measured a grazing incidence signal. Figure 7 shows the placement of the microphones. The primary system used to record the flyover noise containing the source tone was the array of microphones mounted 9.1 m above the ground. There were 10 of these, each separated

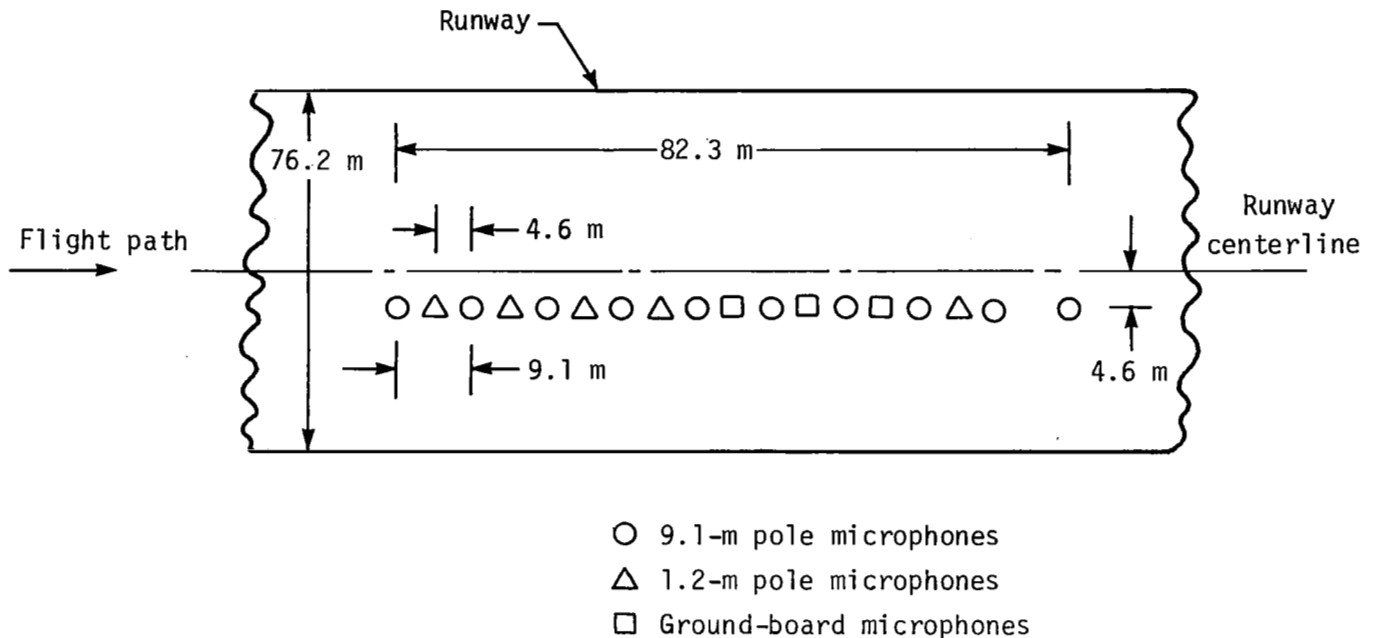


Figure 7.- Diagram of microphone placement for flight-noise measurement.

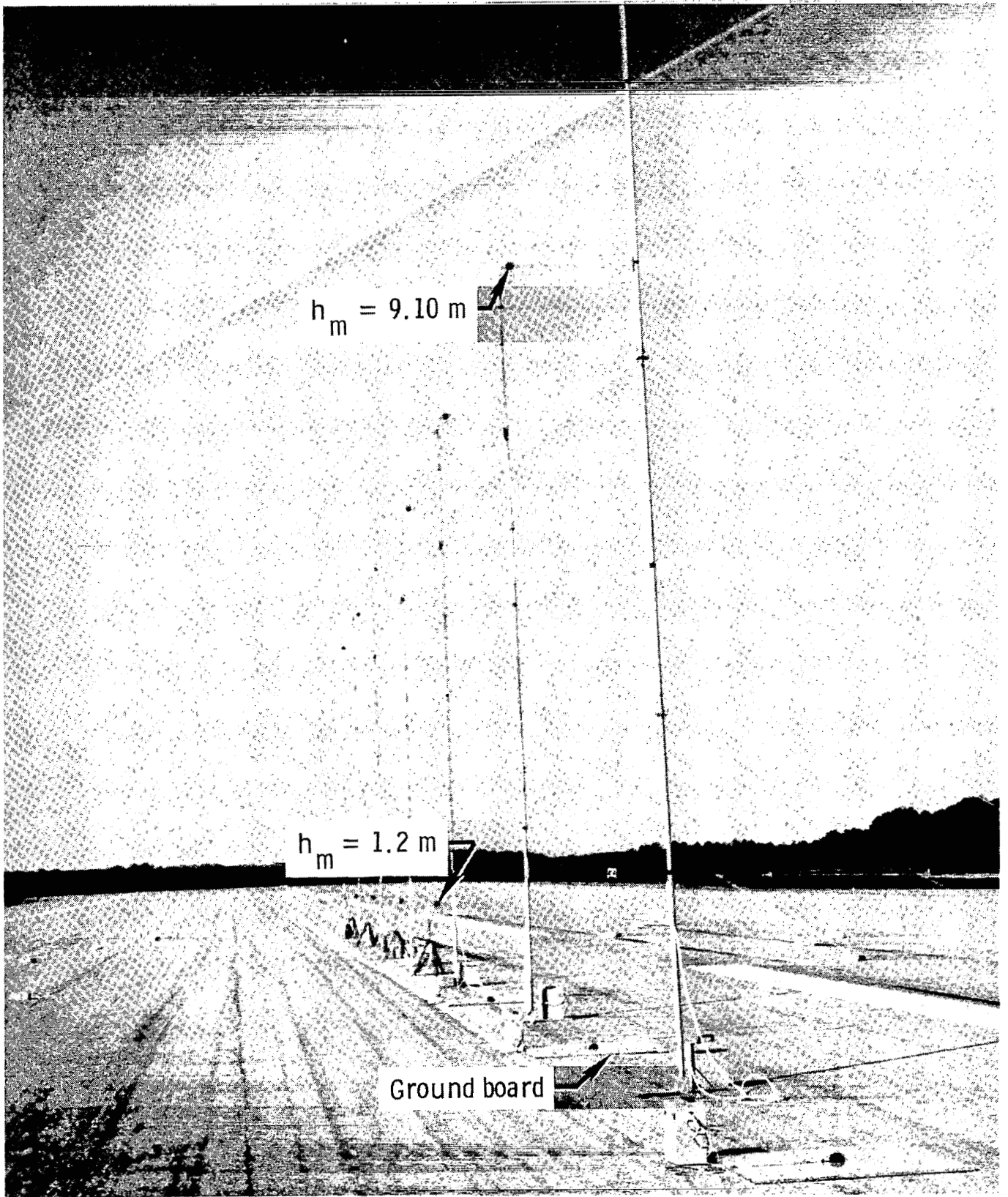
by 9.1 m. Figure 8 presents a photograph showing the microphone setup. Each microphone signal was amplified, high-pass filtered at 500 Hz, and recorded on a 14-channel wide-band analog FM tape recorder.

To document the system's linearity, sensitivity, distortion, and noise floor, each acoustic instrumentation system was laboratory calibrated prior to going into the field. The laboratory calibrations were used to insure that the equipment operated within the manufacturer's specifications. A pistonphone was used in the field each day for sound-level calibration.

Microphone and radar data were correlated by means of a synchronized IRIG A time-code signal which was recorded on each of the data-acquisition systems. The number of microphones used to obtain the data was required as input to the ensemble averaging technique (ref. 7) as described in the appendix.

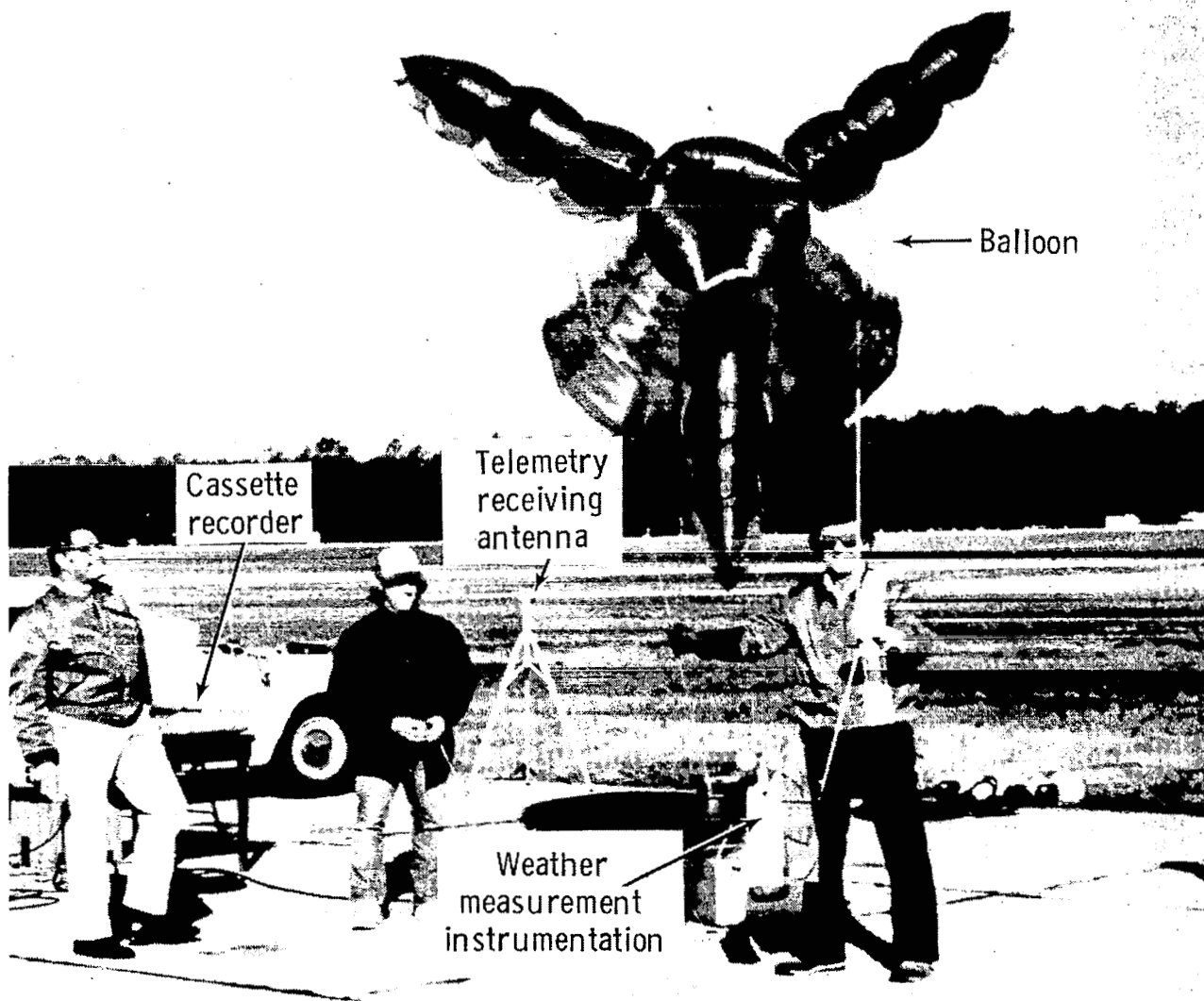
Meteorological system.- A small, tethered, blimp-shaped balloon, with a 4.3 m<sup>3</sup> helium-filled volume, was used to lift instrumentation which provided meteorological data before and during the flight tests. A photograph of the balloon and the weather-measurement system is shown in figure 9. The system includes airborne weather-measurement instrumentation and a ground station comprised of a telemetry receiving antenna, a microcomputer, and a cassette recorder. The instrumentation measured barometric pressure, wind direction, wind speed, temperature, and relative humidity from ground level to an altitude of 100 m.

Results from the meteorological profiles were employed in the data reduction for post-flight analysis and are described in the appendix.



L-81-208

Figure 8.- Array of microphones for flyover noise measurements.



L-81-209

Figure 9.- Weather-measurement system.

## DATA RESULTS AND DISCUSSION

### Outdoor Anechoic Test

Figure 10 shows the results of the first phase of the experiment. This phase, conducted outdoors, measured the far-field radiation pattern of the 4-kHz-source tone. The data, measured 4.6 m from the exit plane of the source, are for angles from  $20^{\circ}$  to  $110^{\circ}$  which represent the flight arc. During each radiation-pattern measurement, the source sound-pressure level remained constant. Radiation patterns were obtained for three source levels. These data were obtained to determine source radiation-pattern shape repeatability and to verify that source-level increases of 6 dB resulted in far-field level increases of 6 dB. A smooth curve was faired through the measured data of figure 10. The curves, plotted on a large scale, indicate that the shape was constant ( $\pm 1$  dB about the smooth curve) for different source strengths, and that the radiation-pattern levels generally increased 6 dB as the source strength was increased 6 dB.

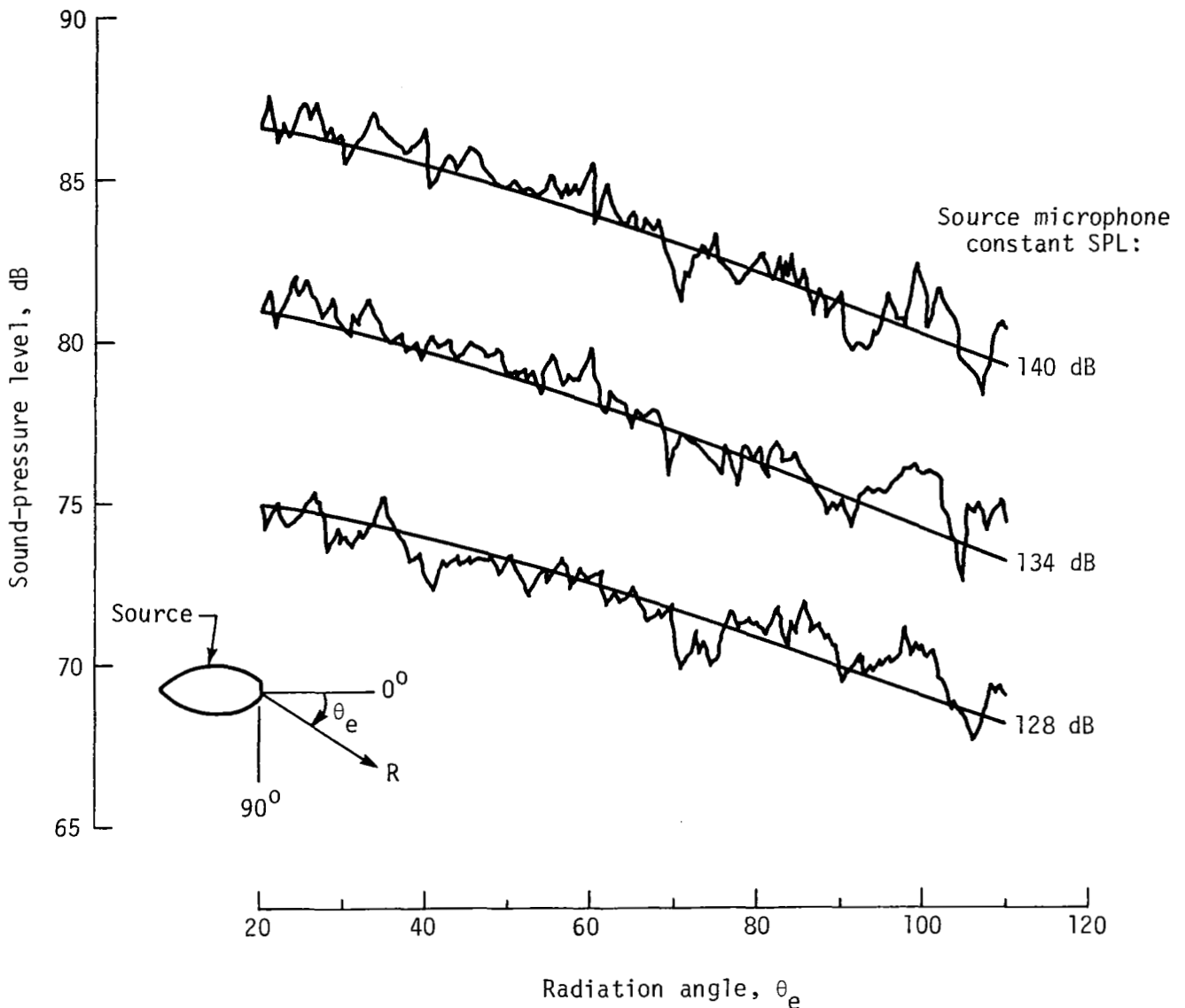
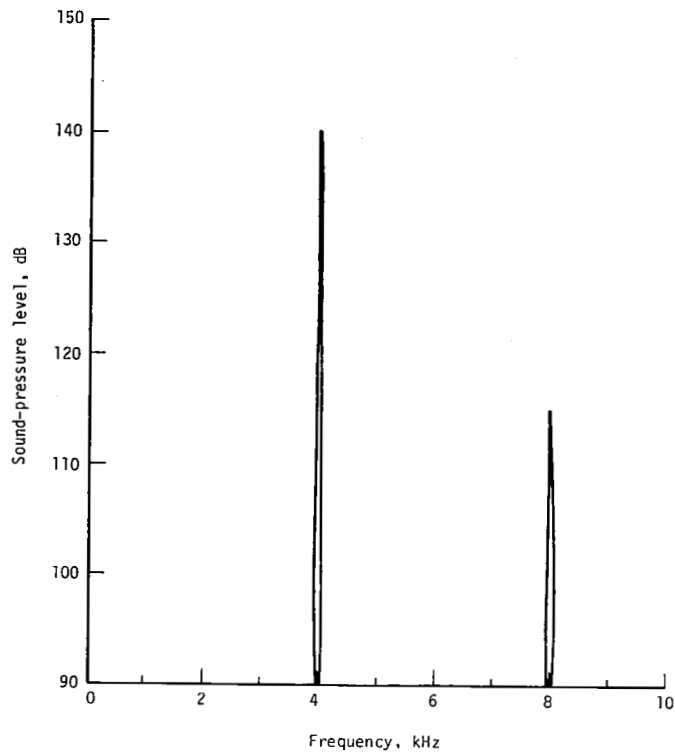


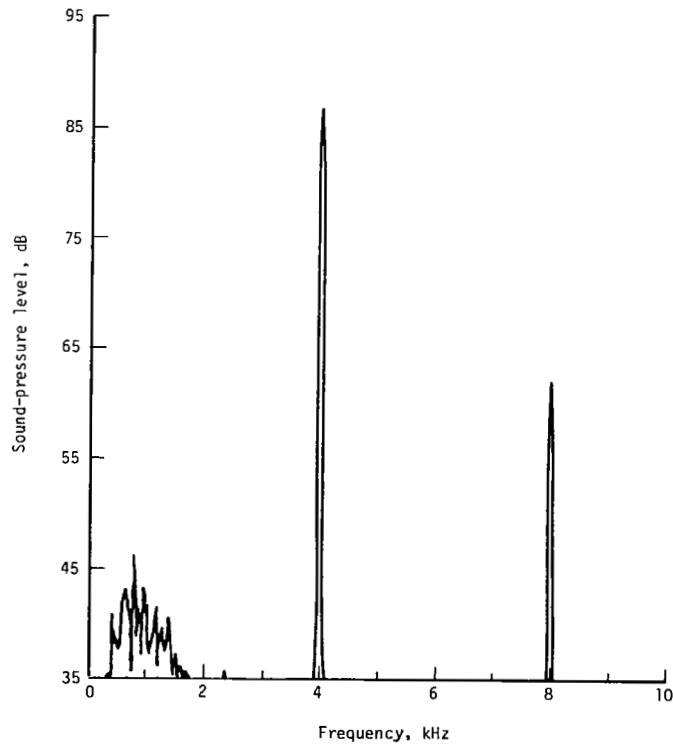
Figure 10.- Measured static far-field radiation pattern at the outdoor anechoic test area.  $R = 4.6$  m.

Figure 11(a) shows the sound pressure levels of the source frequency and its harmonic as measured in the cylindrical tube attached to the acoustic driver. These levels are for the maximum voltage input to the source. The data were measured by the source monitoring microphone and indicate a sound-pressure level of 140 dB at the input fundamental frequency of 4 kHz. The harmonic is 25 dB below this. Figure 11(b) shows for comparison, the amplitudes of this signal and the harmonic measured by the 4.6-m far-field traversing microphone located on the longitudinal axis of the source ( $\theta = 0^\circ$ ). This figure indicates that the harmonic is also 25 dB below the received 4 kHz signal.





(a) Measured in cylindrical tube of acoustic driver.



(b) Measured in far field.  $\theta = 0^\circ$ ;  $R = 4.6$  m.

Figure 11.- Narrow-band (50 Hz) harmonic content of the 4-kHz pure-tone acoustic source.

### Anechoic Flow Test

The next phase of the experiment was to place the acoustic source in an airflow. The Langley Aircraft Noise Reduction Laboratory has the capability of permitting acoustic measurements in an anechoic environment with airflow moving past the noise source.

This phase was conducted in order to determine if the acoustic impedance of the source changed significantly with airflow over it. Although the facility could reach a maximum speed of only one-half the desired flight speeds, these data should indicate any trend aircraft speed might have on the source levels. The data presented in figure 12 indicate that as the air speeds were increased from no-flow conditions to 35 m/s the measured horn-throat sound levels did not change. This indicated that the source impedance did not change.

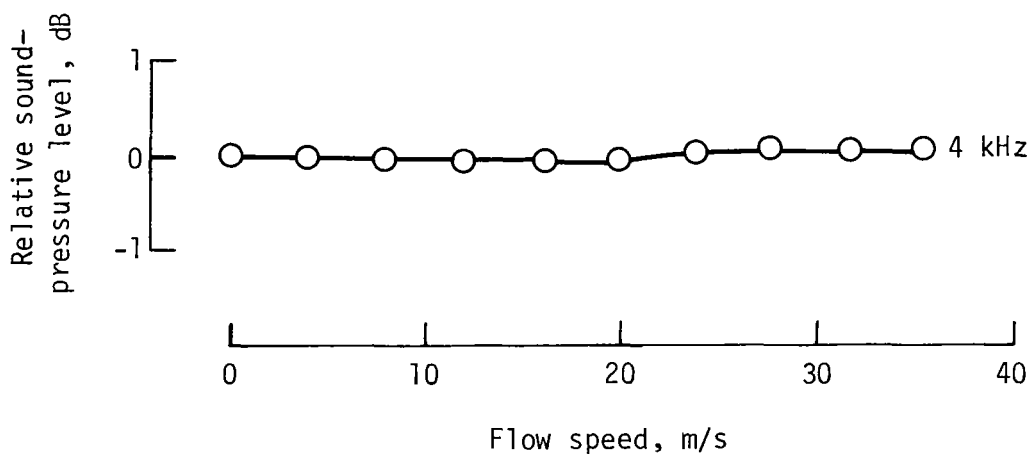
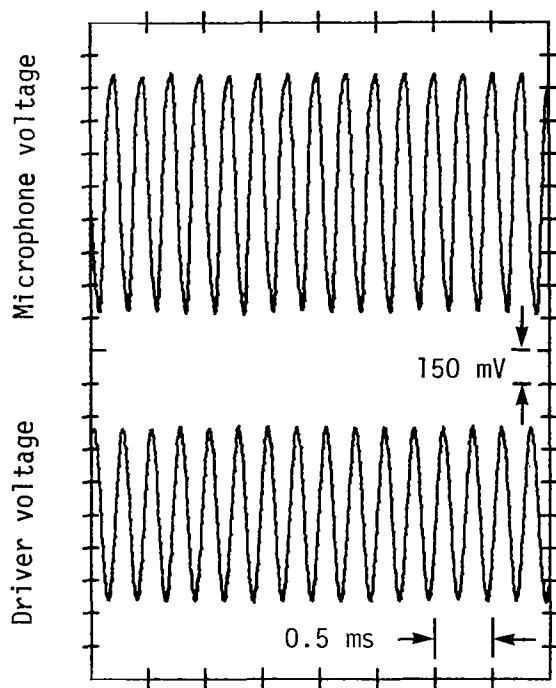


Figure 12.- Effect of flow on sound-pressure level of source microphone.

### Flight Test

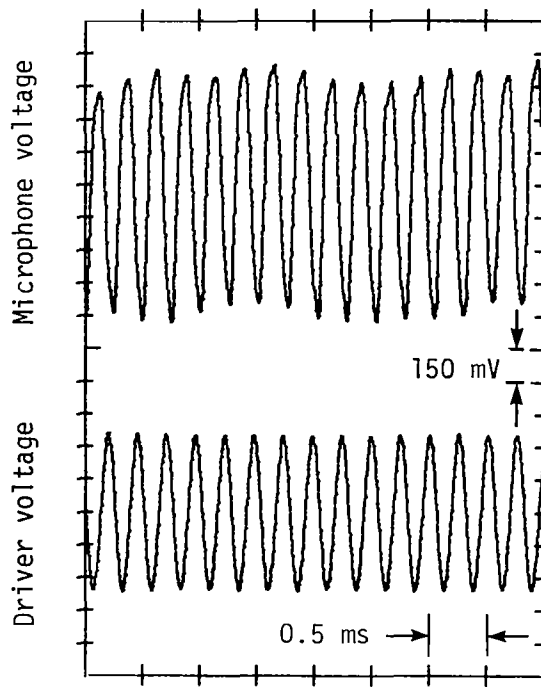
The last phase of the experiment consisted of measuring the far-field acoustic levels of the source as it was flown over the primary microphone array. These measurements were obtained so that the flight radiation pattern of the 4-kHz tone could be converted to a static case and compared to the measured static radiation pattern. As mentioned previously, the flight-to-static conversion required several other measurements. These included the aircraft position and speed relative to the microphone array, the source microphone sound-pressure levels during flight, and the weather data (in 10 m increments from ground level to flight altitude). These measurements were recorded on analog or digital magnetic tape and later reduced and analyzed. The details of the data reduction are found in the appendix, with results presented in figures 13 to 19.

Figure 13 compares the results of the source-input and source-output voltage levels measured statically and in flight. The source level was 140 dB and the flight speed was approximately 70 m/s. The aircraft was in level flight at an altitude of 91 m. The data show the magnitude of the source levels in flight to be the same as those measured statically on the ground. This reinforces the results obtained in the anechoic-flow test shown in figure 12.



Time, sec

Static



Time, sec

Flight

Figure 13.- Comparison of source-input and source-output voltage levels measured statically and in flight at source microphone level of 140 dB.

The weather balloon was flown before and during the acoustic data flights. As discussed earlier, the balloon carried instrumentation which measured the temperature, pressure, relative humidity, wind speed, and wind direction. These were measured in increments of 10 m from the ground to an altitude of 100 m. These measurements were obtained in order to compute the effects of atmospheric absorption. The weather data were studied during acquisition to insure that no temperature or relative humidity inversions existed and that wind speeds were less than 5 m/s (10 knots). Figure 14 presents the weather profiles obtained during the three-day test period. The data indicate that very good weather prevailed for the tests, with the temperatures, relative humidity, and wind speeds showing little change as a function of altitude.

Some typical results of the noise measured at the 9.1-m pole-mounted microphones during a flyover of the source are presented in figure 15. This figure shows narrow band (97 Hz) spectra measured for the source in level flight, at an altitude of approximately 91 m, and for angular positions of 40°, 60°, 80°, 100°, and 110° relative to the microphone array. The data have been ensemble averaged over the microphone array by the technique described in the appendix. The flight speed over the array was about 50 m/s. The data, corrected only for instrumentation effects (see appendix) also show the background noise of the flight environment. This background noise represents the OV-1B spectra with the acoustic source turned off.

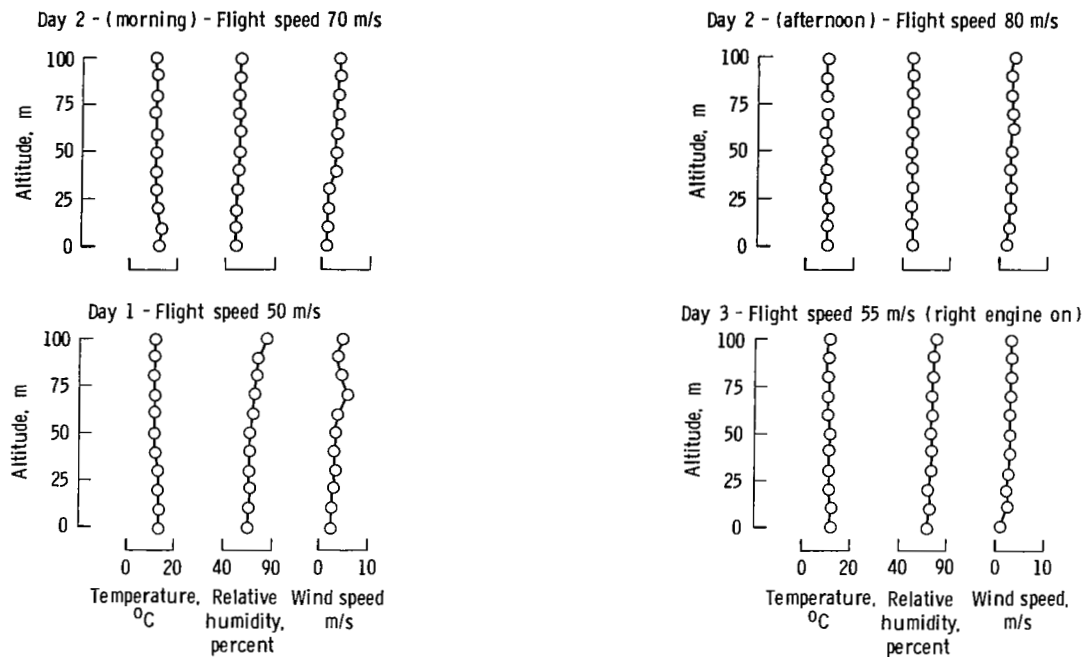


Figure 14.- Weather profiles from ground level to aircraft flight altitude.

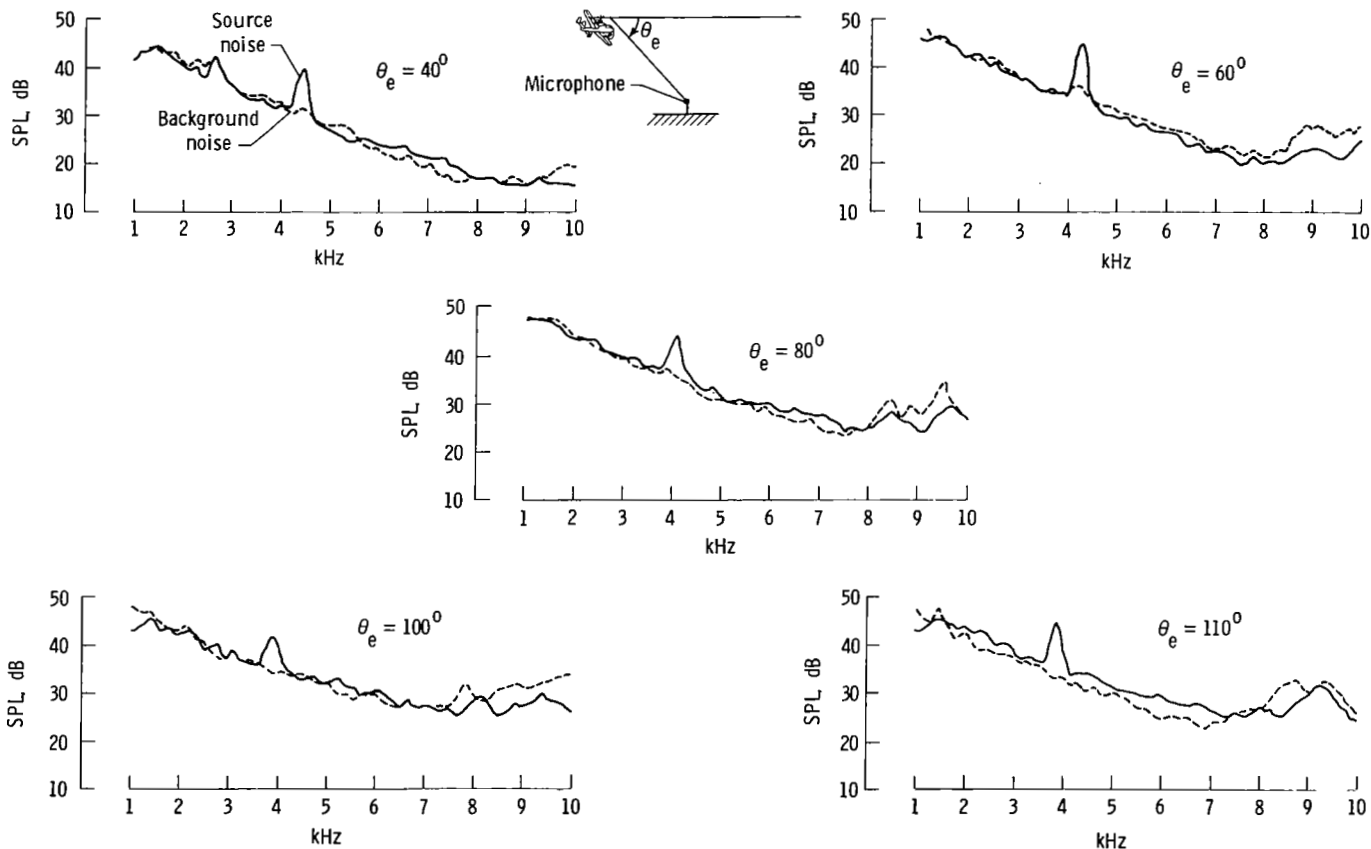


Figure 15.- Narrow-band (97 Hz) flyover noise measurement of source for different emission angles.

Several interesting observations of the data may be made. First, there is a good signal to background noise ratio (about 10 dB) for the 4 kHz tone. The tone also clearly exhibits the expected Doppler frequency shift as the source passes over the microphone array. The shift moves from about 4500 Hz at  $40^\circ$  to about 3800 Hz at  $110^\circ$ . Another observation is that the received tone appears spread over several frequency bands. This is due to the motion of the source and the finite time required to analyze the signal.

There is a high degree of statistical confidence in the magnitudes of the data in figures 15 to 19. All of the acoustic data were ensemble averaged over 8 microphones, which produced a chi-squared 90-percent confidence interval from 1.0 dB to -1.2 dB.

The data of figure 15 represent the first step in the process of obtaining a flight radiation pattern. As discussed earlier, the purpose of this experiment was to measure a flight radiation pattern, convert it to a static case, and compare this to the measured static radiation pattern. The conversion process, discussed in the appendix, consisted of applying numerous corrections to the narrow-band spectra. These corrections removed the effects of instrumentation (ref. 8), background noise (ref. 9), inverse square law (ref. 10), atmospheric absorption (corrected to a lossless condition, ref. 11), convective amplification (ref. 10), and ground impedance (ref. 12). A Doppler correction (ref. 10) was applied to the frequency to account for frequency shifts due to flight. After the flight spectra were corrected, the 4 kHz sound-pressure levels were plotted to obtain the flight-to-static radiation patterns.

Figure 16 shows the cumulative effects of applying each of these corrections to convert from the flight to the static radiation case. Data are presented every  $5^\circ$  from  $20^\circ$  to  $110^\circ$ . It can be seen that the largest corrections are due to

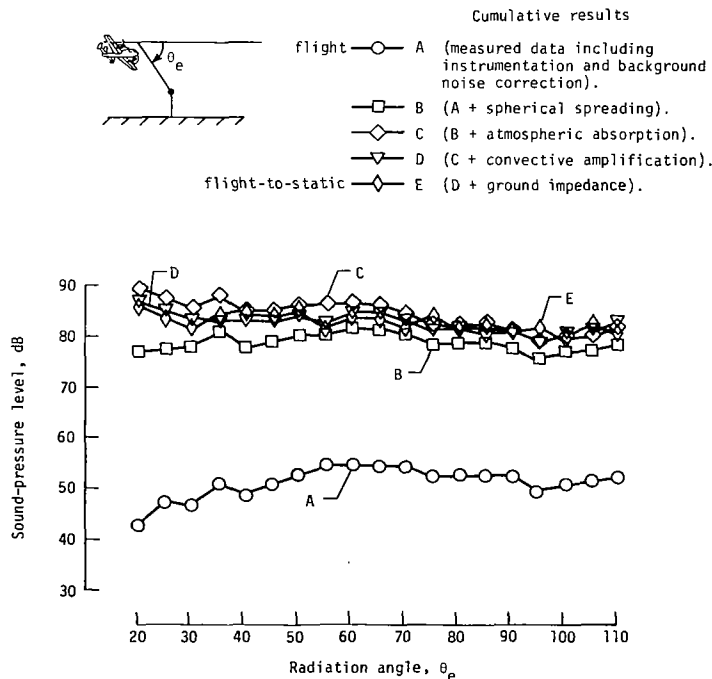


Figure 16.- Comparison of flight-to-static correction values.

spherical spreading (the data were corrected back to the static distance of 4.6 m), with the next largest due to the atmospheric absorption. Both of these are directly related to the propagation path length. The smallest corrections (totaling about 0.5 dB) are due to the instrumentation and the background noise.

The two corrections about which the least may be understood are the effects due to the convective amplification (ref. 13) and ground impedance (ref. 12). The correction model chosen to represent the convective amplification assumes the textbook case of a monopole source in motion (ref. 10). The ground impedance correction was modeled assuming a perfectly hard reflecting surface.

Data analysis showed that the tone energy received at the microphones appeared to be spread evenly over two contiguous bands of analysis. In order to account for this and arrive at a representative level of the source tone, it was decided to add the mean-square pressures in the band containing the 4-kHz tone with those levels in the adjacent band (depending on aircraft angular location). This has the same effect as performing a narrow-band analysis of about 200 Hz. A further discussion of this procedure appears in the appendix.

Figure 17 shows the results of converting one set of the radiation data measured in the flight experiment to the equivalent static radiation case and comparing it to the measured static radiation pattern. In each case the source level was 140 dB.

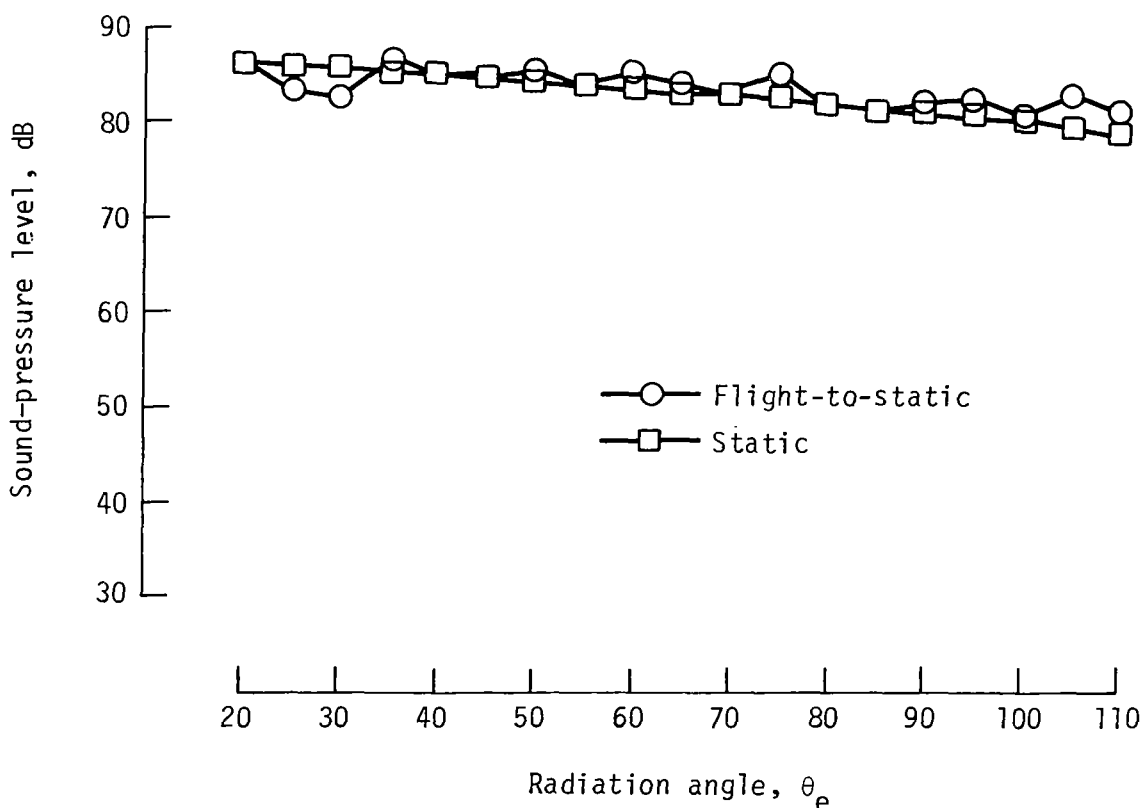


Figure 17.- Comparison of 4-kHz radiation pattern of flight-to-static results and static results.

The flight data represent level flight at 91 m at a speed of about 50 m/s. It can be seen that over the angular range of  $20^\circ$  to  $110^\circ$ , the flight-to-static case comes within  $\pm 3$  dB of the static data. The best agreement between the curves is between  $40^\circ$  to  $100^\circ$ . These results indicate that the measurement and analytical procedures are valid.

A total of four sets of flight data were obtained. Three sets of data were obtained for the aircraft flying in level flight (91 m altitude) at speeds of about 50, 70, and 80 m/s. In each case the right engine was shut down and the flaps and gear were retracted. The fourth set of data was obtained for level flight at 91 m altitude and a speed of about 55 m/s. In this case, the right engine was at the same operational setting as the left engine. The landing gear was down and the flaps were extended  $15^\circ$ .

The purpose of the first three sets of flight data was to determine if there were any speed effects on the radiation pattern. Figure 18 shows these results. Two observations may be made about the data. The first is that the shape of the overall

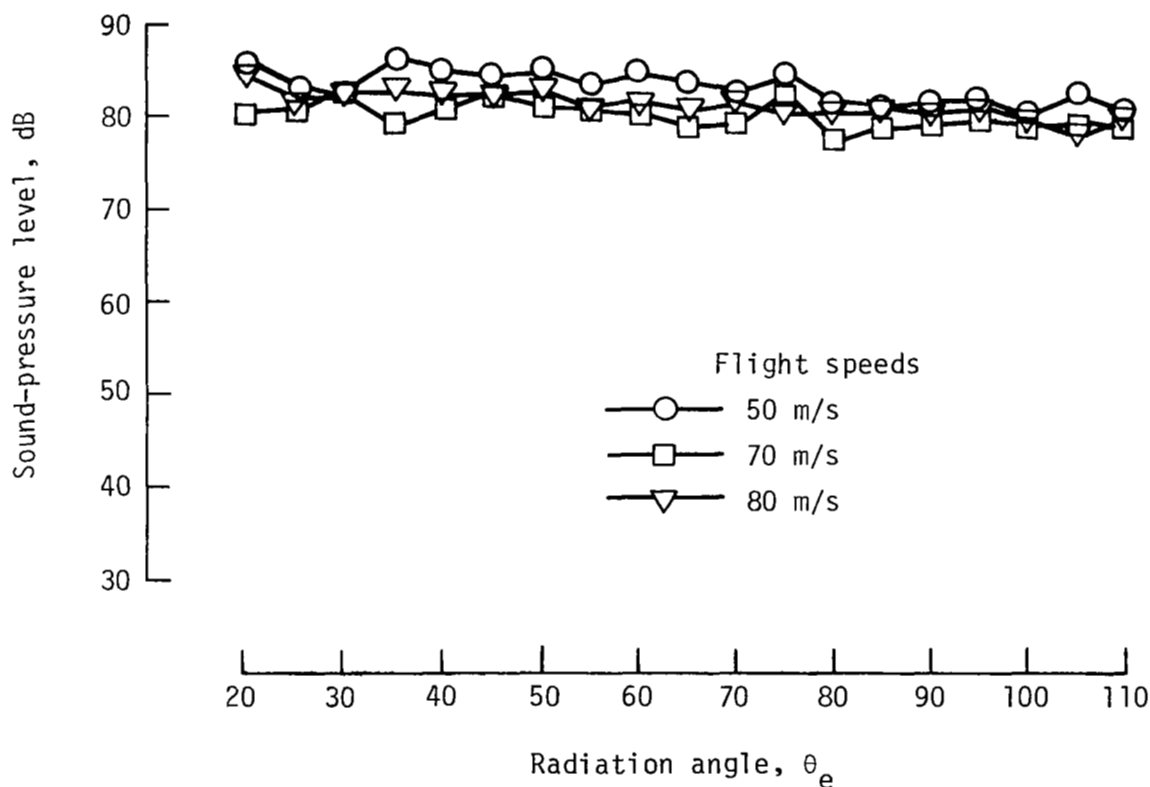


Figure 18.- Comparison of flight-to-static radiation patterns for three flight speeds.

radiation pattern did not change significantly for the three flight speeds. The other observation is that there seems to be no trend toward reduced acoustic levels with increasing flight speed. In general, for the three flight speeds, the levels of

the radiation patterns were repeatable within  $\pm 3$  dB. The largest variation tends to occur at the shallow angles of propagation with the least variation occurring when the source was closest to the microphones ( $\theta_e = 90^\circ$ ). These data appear to fall within the range of experimental error and suggest good repeatability of the radiation pattern.

The purpose of the fourth set of data was to determine if there were any effects on the source due to the operation of the right engine on the aircraft. The test was conducted under conditions that are expected to apply to a future flight-effects program. Figure 19 compares the flight-to-static data of figure 17 (flight speed of 50 m/s) to the flight-to-static radiation pattern obtained when the right engine was operating at the same conditions as the left engine. With both engines operating to

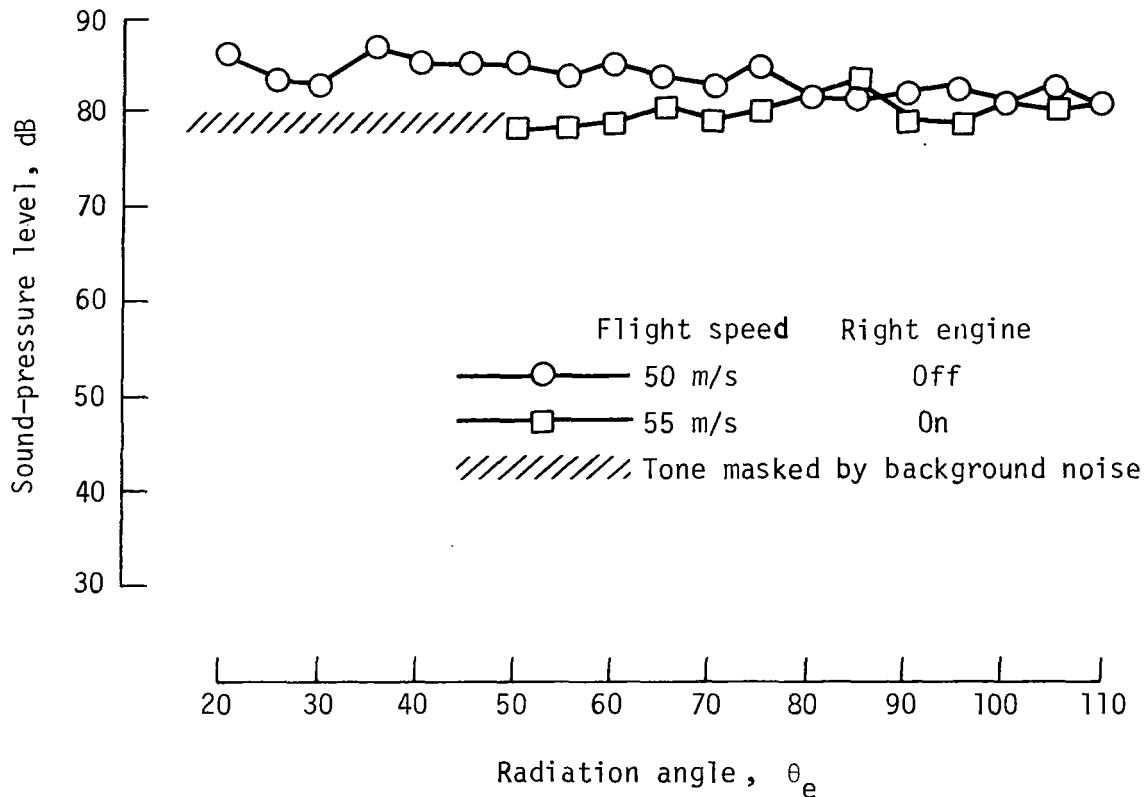


Figure 19.- Comparison of flight-to-static radiation pattern for right engine off and on.

maintain a constant flight speed of about 55 m/s at an altitude of 91 m, the landing gear was extended and the flaps were set to  $15^\circ$ . The signal-to-noise ratios for this flight case were not as high as the previously discussed flights. At  $\theta$  values less than  $50^\circ$ , the aircraft background noise masked the source noise and the 4-kHz tone was not observed. The sound-pressure levels at values of  $\theta$  greater than  $50^\circ$  were generally between 3 dB and 6 dB above the aircraft noise with the signal-to-noise ratio increasing as  $\theta$  increased (i.e., as the propagation path to the microphone decreased). These signal-to-noise ratios were less than desirable for the experiment. From  $50^\circ$  to about  $70^\circ$ , the data from this flight case appear somewhat lower than the data taken with the right engine off. From  $70^\circ$  to  $110^\circ$ , the data are compatible with those taken with the right engine off. The high background noise at



shallow angles less than  $50^\circ$  and the low source sound-pressure levels from  $50^\circ$  to  $70^\circ$  are believed to be due to the operating right engine and a scattering of the source noise by the rotating propeller of this engine.

#### CONCLUDING REMARKS

A pure-tone acoustic source (4 kHz) was flown at a constant altitude and under different aircraft operating conditions over a linear array of microphones. The flyover noise-radiation patterns were determined and compared to the measured static radiation pattern of the source. This was accomplished by first establishing a flyover-noise data-reduction system which merged large quantities of accurate laser-radar tracking data with acoustic and weather data. The nonstationary acoustic flight data were reduced to a representation of stationary data by short integration times in the fast Fourier transform and ensemble averaging over eight microphones. These techniques produced narrow-band spectra with a chi-squared 90-percent confidence interval of about  $\pm 1$  dB.

The flyover-averaged acoustic spectral data were adjusted to the static case by correcting for the effects of instrumentation, background noise, inverse square law, atmospheric absorption, convective amplification, ground impedance, and Doppler frequency shift. The corrected sound-pressure levels of the source tone in the spectra were then plotted as a function of angle to produce the flight-to-static radiation pattern. Results showed excellent agreement over the angular range from  $20^\circ$  to  $110^\circ$ . The patterns agreed to within  $\pm 3$  dB over the angular range.

The 4-kHz-tone radiation pattern seemed not to be a function of flight speed over the range of 50 to 80 m/s and there seemed to be no installation effects while the right engine was shut down. When the right engine was operating, the radiation-pattern sound levels were adversely influenced, especially at shallow radiation angles.

Langley Research Center  
National Aeronautics and Space Administration  
Hampton, VA 23665  
August 7, 1981

## APPENDIX

### FLIGHT-TO-STATIC DATA REDUCTION TECHNIQUE

The components of the data acquisition and reduction package are indicated in table I. Listed are the data-acquisition systems, their source formats, measured parameters, and the preliminary results. These preliminary results were merged into a large computer data file. This data file was then corrected as required and analyzed for trends in the source spectra and radiation pattern.

#### Radar System

The radar system uses an FPS-16 radar in conjunction with a laser. The FPS-16 initially acquires the aircraft in flight, then accurately ( $\pm 0.15$  m) locates it through the use of a laser which tracks a reflecting laser cube located on the nose of the aircraft. A digital magnetic tape is used to store the raw aircraft-position time histories relative to the microphone array. Since these data are for the laser cube, and the noise source is located on the right wing, the data are converted by a linear transformation of Cartesian coordinates to represent the source position, speed, and time of emission relative to the microphone array. These data are then merged with the acoustic and weather information.

#### Acoustic System

The acoustic data system consisted of the microphone layout discussed earlier (fig. 8). This system consisted of an analog magnetic tape recorder which recorded the source-noise time histories. For the purpose of this experiment, 10 acoustic data channels were used. After the analog acoustic data were obtained, these 10 data channels were digitized using a sample rate of 50 000 points per second.

#### Time Shifting

The data for microphones 2 to 10 were then time shifted so that spectra could be related to the source position ( $R_e, \theta_e$ ) and emission time  $t_e$  relative to microphone 1. This was accomplished in the following manner. Figure 20 schematically represents the aircraft flyover of a microphone array. For any given source location ( $R_e, \theta_e$ ) at a moment in time relative to microphone one, each noise data channel is related to the first microphone signal by a time  $\tau_m$  where

$$\tau_m = \frac{nd}{v}$$

where

$n = 2, 3, \dots, 10$  for the 2nd, 3rd,  $\dots$ , 10th microphone

$d = 9.1$  m (30 ft) spacing between microphones

$v =$  Speed of the aircraft over the array

APPENDIX

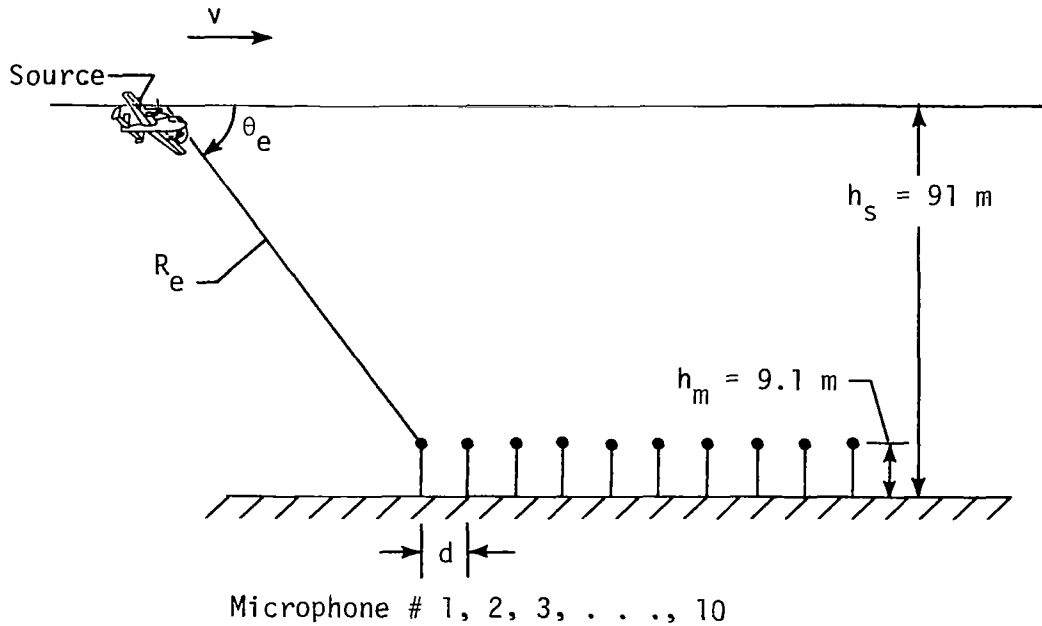


Figure 20.- Aircraft flyover of a multiple microphone linear array.

Thus, by shifting the noise data channels 2 to 10 by an amount of time  $\tau$  for each channel, the noise emission time and position location described by  $\theta_e^m$  and  $R_e$ , relative to microphone 1, are directly related to all the acoustic data channels.

Once the times for microphones 2 to 10 were shifted, it was then necessary to merge them with the source emission times from the radar data file. This permitted the received acoustic signal to be identified with the source location. This was accomplished by recognizing that the time required for the source noise to travel the propagation path  $R_e$  (obtained from radar data) to the microphone is given

by  $\frac{R_e}{c}$  where  $c$  is the speed of sound along the path. The noise signal received on the analog tapes at the moment in time  $t_r$  is related to the source emission time  $t_e$  by the expression

$$t_e = t_r - \frac{R_e}{c}$$

The speed of sound was calculated using the expression

$$c = 331.6 \left( \frac{T}{T_0} \right)^{1/2}$$

where

$$T = 273.15 + t$$

## APPENDIX

$t$  = Mean temperature measured by weather system in centigrade degrees from ground to aircraft altitude

$T_0 = 293.15$  K (ref. 11)

After the time shifting and source emission time and location procedures were performed, the data were then operated on by a fast Fourier transform (FFT) process to produce narrow band (97 Hz) spectra for each of the acoustic data channels. These preliminary results are indicated in the last column of table I. These spectra were then ensemble averaged to improve the statistical accuracy of the sound-pressure levels.

### Ensemble Averaging

In order to obtain a high resolution of the source location as it flew over the microphone array, time increments of 0.01 s were used in the FFT process to obtain acoustic spectra. Thus, it was possible to accurately indicate where the aircraft was for an associated spectrum. Another benefit of using a short integration time was to try and reduce the energy smearing across frequency bands of the received noise signal which occurs due to the motion of the aircraft. A major drawback of these short integration times is a poor estimate of the pressure level. In order to maintain the position resolution in this experiment and obtain high statistical confidence levels of the measured sound levels, the technique of time-segment and ensemble averaging discussed by Bendat and Piersol (ref. 7) was employed.

Table II shows the chi-squared 90-percent confidence values for the degrees of freedom associated with the integration times (0.01 s and averaged over 5 time segments) and number of microphones used in this experiment. A level of approximately  $\pm 1$  dB was desired. As shown, this could be obtained by averaging over 8 to 10 microphones. Throughout the experiment there were always eight microphones which functioned well, thus it was decided to perform the averages over eight microphones for a 90-percent confidence level from 1 dB to -1.2 dB.

Once the acoustic data were averaged and related to the source location ( $\theta_e, R_e$ ), the acoustic spectra were obtained over the range  $20^\circ < \theta_e < 110^\circ$ . These data were then corrected for instrumentation and propagation effects.

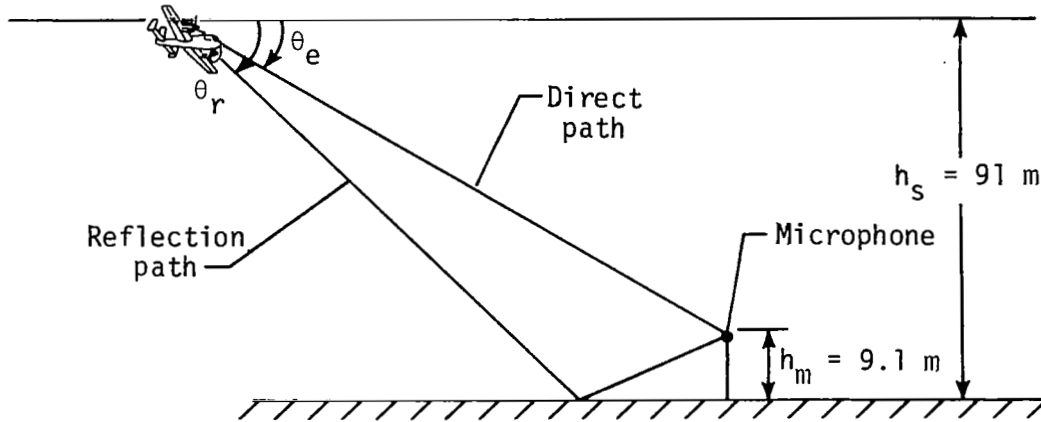
### Weather System

In order to correct the acoustic data for the affects of the atmosphere, the weather data system (fig. 9) indicated in table I was used. This system consisted of a large balloon flown on a tether. Suspended beneath the balloon was an instrumentation package which measured the atmospheric pressure, temperature, wind speed, wind direction, and relative humidity. Each data point was sampled every 10 m from the ground to 100 m and telemetered to the ground. The data were recorded on a digital cassette recorder as the balloon ascended to the flight altitude. After the flights, the tapes were removed from the digital cassettes and altitude profiles indicated in the last column of table I were obtained. These weather data were then placed in a large computer data file so that the weather corrections, along with other corrections, could be applied.

APPENDIX

Correction Procedure

Both instrumentation and propagation corrections were applied to the ensemble-averaged acoustic spectra. These corrections are indicated in figure 21.



<u>Instrumentation</u>	<u>Propagation path</u>
1. Microphone response	1. Inverse square law
2. Microphone diffraction effects	2. Atmospheric absorption
3. Windscreen insertion loss	3. Convective amplification
4. System response	4. Ground impedance
	5. Doppler frequency shifts
	6. Background noise

Figure 21.- Corrections applied to measured acoustic flight data.

The first set of corrections applied to the spectral data were those associated with the instrumentation. Table III lists the values used for the microphone response, diffraction, and windscreen effects. These values were obtained from laboratory calibrations, manufacturers literature, and from a laboratory study (ref. 8). System-response corrections are not listed as they were 0 dB from 1 kHz to 10 kHz.

The second set of corrections were associated with the propagation path. Standard methods were followed in applying the corrections for the background noise (ref. 9), inverse square law (ref. 10), Doppler frequency shift (ref. 11), and atmospheric absorption (corrected to lossless conditions, ref. 11). The atmospheric absorption was computed by dividing the atmosphere into ten layers, each with its own set of weather data. The absorption coefficient for each layer was computed and applied to the signal as it traversed the propagation path.

## APPENDIX

The complexity of modeling the convective amplification has been presented by Dowling (ref. 13). In the absence of a generally accepted method, the textbook relationship (ref. 10) for a monopole source in motion was used such that

$$p_m = p_s (1 - M \cos \theta_e)^2$$

where

$p_m$  is the sound pressure measured by the microphone

$p_s$  is the sound pressure of the source

$M$  is the Mach number

$\theta_e$  is the propagation path angle

The procedure used to correct for the reflected energy from the ground was that for narrow-band analysis of random noise established by reference 12. Because the source, mixed with flight noise, was in motion and propagated through the atmosphere, the measured signal was treated as being random. The ground was assumed to be perfectly reflecting, which resulted in a 3 dB correction for the narrow-band spectrum of the received signal. It is expected that if impedance models other than a perfectly reflecting surface were chosen, the impedance correction values would fall between about 1.5 dB and 2.5 dB (refs. 14, 15, and 16).

An example of a data listing showing the format of the required corrections and flight information is seen in table IV.

In addition to this ground-impedance correction, an analysis of the flyover data indicated that the spectra seemed to peak in both the band containing the 4 kHz tone and an adjacent band depending on aircraft location. This is due to the motion of the source and the time required to analyze the energy received at the microphone. This spreading of the energy may be explained by considering figure 21 and the Doppler shift equation

$$f_r = f_s (1 - M \cos \theta_e)^{-1}$$

where  $f_r$  is the received frequency. The energy from the source frequency  $f_s$  travels two paths (direct and reflected) to reach the microphone. The direct path is indicated by a value of  $\theta_e$  and the reflected path by  $\theta_r$ . During the analysis time, energy from these two paths arrive at the microphone and are averaged. An additional correction was performed to account for this smearing effect by summing the energy in the two bands which contained the peak sound-pressure levels. This had the effect of increasing the analysis bandwidth to 194 Hz for the 4 kHz tone, and was thought to better represent the source strength.

## REFERENCES

1. Chun, K. S.; Berman, C. H.; and Cowan, S. J.: Effects of Motion on Jet Exhaust Noise From Aircraft, NASA CR-2701, 1976.
2. Atvars, Y.; and Rogers, D. F.: The Development of Inflow Control Devices for Improved Simulation of Flight Noise Levels During Static Testing of a HBPR Turbofan Engine. AIAA-80-1024, June 1980.
3. Beran, D. W.; and Gething, J. T.: Use of a Sailplane in Measuring Acoustic Attenuation in the Atmosphere. Aero-Revue, no. 2., Feb. 1972, pp. 93-95.
4. Norum, T. D.; and Liu, C. H.: Point Source Moving Above a Finite Impedance Reflecting Plane - Experiment and Theory. J. Acoust. Soc. America, vol. 63, no. 4, Apr. 1978, pp. 1069-1073.
5. Hogstedt, C. R.; and Lowder, E. M.: An Airborne Reference Noise Source for Studying Airplane Flyover Noise Propagation and Measurement. AIAA Paper 79-0650, Mar. 1979.
6. Hardin, Jay C.; and Preisser, John S.: Stochastic Analysis of Spectral Broadening by a Free Turbulent Shear Layer. NASA TP-1816, 1981.
7. Bendat, Julius S.; and Piersol, Allan G.: Random Data: Analysis and Measurement Procedures. John Wiley & Sons, Inc., c.1971.
8. Mueller, Arnold W.: A Comparison of the Three Methods Used To Obtain Acoustic Measurements for the NASA Flight Effects Program. NASA TM-81906, 1980.
9. American National Standard Method for the Physical Measurement of Sound. ANSI S1.2-1962 (R1971), American Natl. Stand. Inst., Inc., Aug. 20, 1962.
10. Morse, Philip M.; and Ingard, K. Uno: Theoretical Acoustics. McGraw-Hill Book Co., Inc., c.1968.
11. American National Standard Method for the Calculation of the Absorption of Sound by the Atmosphere. ANSI S1.26-1978 (ASA 23-1978), June 23, 1978.
12. Acoustic Effects Produced by a Reflecting Plane. AIR 1327, Soc. Automat. Eng., Jan. 15, 1976.
13. Dowling, Ann: Convective Amplification of Real Simple Sources. J. Fluid Mech., vol. 74, pt. 3, Apr. 6, 1976, pp. 529-546.
14. Burley, Richard R.; Karabinus, Raymond J.; and Freedman, Robert J.: Flight Investigation of Acoustic and Thrust Characteristics of Several Exhaust Nozzles Installed on Underwing Nacelles on an F106 Airplane. NASA TM X-2854, 1973.
15. Harbour, S. J.: Ground Reflection Effects on Aircraft Flyover Noise. AIAA-80-1059, June 1980.
16. Miles, J. H.: Analysis of Ground Reflection of Jet Noise Obtained With Various Microphone Arrays Over an Asphalt Surface. NASA TM X-71696, [1975].

## SYMBOLS


$c$	speed of sound
$c_{avg}$	average speed of sound
$c_{gi}$	speed of sound for ground impedance measurements
$d$	separation distance between microphones
$f$	frequency
$f_r$	frequency received at microphone
$f_s$	source frequency
$h_m$	microphone height above ground
$h_s$	source height above ground
$M$	Mach number
$P_m$	sound pressure measured by microphone
$P_s$	source sound pressure
$R$	noise propagation path length
$R_e$	noise propagation path length at emission time
$RH$	relative humidity
$SPL$	sound-pressure level
$T$	temperature, K
$T_o$	293.15 K
$t$	temperature, °C
$t_e$	noise emission time
$t_r$	noise reception time
$v$	aircraft speed
$WS$	wind speed
$X, Y, Z$	Cartesian coordinates
$\theta$	noise radiation angle



$\theta_e$  noise radiation angle at emission time  
 $\theta_r$  source radiation angle associated with reflection path  
 $\tau_m$  noise time signal delay between microphones

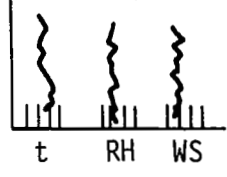
TABLE I.- DATA SYSTEMS USED TO OBTAIN CORRECTED FLYOVER NOISE-REDUCTION PATTERNS

Data system	Source format	Raw parameter	Preliminary results
Radar	Digital magnetic tape	Run identification time - position coordinates	Transformed positioned coordinates
Acoustic	Analog magnetic tape	Noise time histories	Time shifted spectra
Weather	Digital cassette tape	Pressure, temperature, wind speed and direction, relative humidity	Altitude profiles



SPL

f



Altitude

t RH WS

TABLE II.- CHI-SQUARED 90-PERCENT CONFIDENCE LEVELS FOR NUMBER  
OF MICROPHONES USED IN ENSEMBLED AVERAGES

Statistical degree of freedom (0.01 sec averaged over 5 time segments per microphone)	Number of microphones	90-percent confidence levels	
		Lower bound (dB)	Upper bound (dB)
10	1	-4.1	2.6
20	2	-2.8	2.0
30	3	-2.1	1.6
40	4	-1.8	1.4
50	5	-1.6	1.3
60	6	-1.4	1.2
70	7	-1.3	1.1
80	8	-1.2	1.0
90	9	-1.1	1.0
100	10	-1.1	.9

TABLE III.- INSTRUMENTATION CORRECTIONS ADDED TO MEASURED SOUND-PRESSURE LEVELS

Frequency, kHz	Pressure response, dB	Diffraction, dB	Windscreen, dB	Frequency, kHz	Pressure response, dB	Diffraction, dB	Windscreen, dB
1.0	0	0.1	0	8.0	-1.0	0.4	0.5
1.1	↓	↓	↓	8.1	↓	↓	.5
1.2	↓	↓	↓	8.2	↓	↓	.5
1.3	↓	↓	↓	8.3	↓	↓	.8
1.4	↓	↓	↓	8.4	↓	↓	↓
1.5	↓	↓	↓	8.5	-1.2	↓	↓
1.6	↓	↓	↓	8.6	↓	↓	↓
1.7	↓	↓	↓	8.7	↓	↓	↓
1.8	↓	↓	↓	8.8	↓	↓	↓
1.9	↓	↓	-.3	8.9	↓	↓	↓
2.0	0	0.2	-0.3	9.0	-1.3	0.4	0.8
2.1	↓	↓	↓	9.1	↓	↓	↓
2.2	↓	↓	↓	9.2	↓	↓	↓
2.3	↓	↓	↓	9.3	↓	↓	↓
2.4	↓	↓	0	9.4	↓	↓	↓
2.5	↓	↓	0	9.5	↓	↓	↓
2.6	↓	↓	-.5	9.6	↓	↓	↓
2.7	↓	↓	↓	9.7	↓	↓	1.0
2.8	↓	↓	↓	9.8	↓	↓	1.0
2.9	↓	↓	↓	9.9	↓	↓	1.0
3.0	0	0.2	-0.5	10.0	-1.3	0.4	1.0
3.1	↓	↓	↓	10.1	↓	↓	↓
3.2	↓	↓	↓	10.2	↓	↓	↓
3.3	↓	↓	-.3	10.3	↓	↓	↓
3.4	-.2	↓	0	10.4	↓	↓	↓
3.5	-.3	↓	↓	10.5	↓	↓	↓
3.6	↓	↓	↓	10.6	↓	↓	↓
3.7	↓	↓	↓	10.7	↓	↓	↓
3.8	↓	↓	↓	10.8	↓	↓	↓
3.9	↓	↓	↓	10.9	↓	↓	.5
4.0	-0.3	0.2	0	11.0	-1.3	0.4	0.8
4.1	↓	↓	.3	11.1	↓	↓	↓
4.2	↓	↓	.5	11.2	↓	↓	↓
4.3	↓	↓	↓	11.3	↓	↓	↓
4.4	↓	↓	↓	11.4	↓	↓	.5
4.5	-.4	↓	↓	11.5	↓	↓	1.0
4.6	↓	↓	↓	11.6	↓	↓	↓
4.7	↓	↓	↓	11.7	↓	↓	↓
4.8	↓	↓	↓	11.8	↓	↓	↓
4.9	.5	↓	↓	11.9	↓	↓	↓
5.0	-0.5	0.3	0.5	12.0	-1.3	0.4	1.0
5.1	↓	↓	↓	12.1	↓	↓	↓
5.2	↓	↓	↓	12.2	↓	↓	↓
5.3	↓	↓	↓	12.3	↓	↓	↓
5.4	↓	↓	↓	12.4	↓	↓	↓
5.5	-.5	↓	↓	12.5	↓	↓	↓
5.6	↓	↓	↓	12.6	↓	↓	↓
5.7	↓	↓	↓	12.7	↓	↓	↓
5.8	↓	↓	↓	12.8	↓	↓	↓
5.9	↓	↓	↓	12.9	↓	↓	↓
6.0	-0.5	0.3	0.5	13.0	-1.3	0.5	1.0
6.1	↓	↓	.5	13.1	↓	↓	1.0
6.2	↓	↓	.3	13.2	↓	↓	1.3
6.3	-.6	↓	0	13.3	↓	↓	1.5
6.4	-.6	↓	↓	13.4	↓	↓	↓
6.5	-.7	↓	↓	13.5	↓	↓	↓
6.6	↓	↓	↓	13.6	↓	↓	↓
6.7	↓	↓	↓	13.7	↓	↓	↓
6.8	↓	↓	↓	13.8	-1.0	↓	↓
6.9	↓	↓	↓	13.9	-1.0	↓	1.8
7.0	-0.9	0.3	0	14.0	-1.0	0.5	1.5
7.1	↓	↓	↓	14.1	↓	↓	↓
7.2	↓	↓	↓	14.2	↓	↓	↓
7.3	↓	↓	↓	14.3	↓	↓	↓
7.4	↓	↓	↓	14.4	↓	↓	↓
7.5	-.9	↓	↓	14.5	-1.0	↓	1.3
7.6	↓	↓	↓	14.6	↓	↓	1.0
7.7	↓	↓	↓	14.7	↓	↓	1.0
7.8	↓	↓	.3	14.8	↓	↓	1.5
7.9	↓	↓	.5	14.9	↓	↓	1.5

TABLE IV.- TYPICAL DATA LISTING AND CORRECTIONS FOR AIRCRAFT FLYOVER NOISE

Averaged over 8 microphones and 5 time segments.  $t_e = 60\ 528\ s$ ;  
 $R_e = 85.34\ m$ ;  $\theta_e = 75^\circ$ ;  $v = 69.07\ m/s$ ;  $X = -24.65\ m$ ;  
 $Y = 7.22\ m$ ;  $Z = 84.95\ m$ ;  $c_{avg} = 337.99\ m/s$ ;  $c_{gi} = 338.75\ m/s$ ;  
 $M = 0.20$

CODE FOR CORRECTIONS MADE:  
 IC=INSTRUMENTATION  
 CA=CONVECTIVE AMPLIFICATION  
 IS=INVERSE SQUARE LAW  
 AA=ATMOSPHERIC ABSORPTION  
 GI=GROUND IMPEDANCE  
 DF=DOPPLER FREQUENCY SHIFT

FREQUENCY	AVG SPL, DB	DELTA SPL (IC)	DELTA SPL (CA)	DELTA SPL (IS)	DELTA SPL (AA)	DELTA SPL (GI)	FREQUENCY (DF)	AVG SPL, DB FINAL
0.0000	38.3359	0.0000	-0.9441	-25.4210	0.0000	3.1887	0.0000	59.6241
97.6562	37.2208	.0000	-.9441	-25.4210	.0240	3.0445	92.4907	58.6772
195.3125	36.4795	.0000	-.9441	-25.4210	.0682	2.8926	184.9814	58.1321
292.9688	44.7353	.0000	-.9441	-25.4210	.1067	2.9629	277.4721	66.3561
390.6250	50.8364	.0000	-.9441	-25.4210	.1382	3.0391	369.9628	72.4123
488.2813	53.9218	.0000	-.9441	-25.4210	.1666	3.0267	462.4536	75.5386
585.9375	53.5186	.1000	-.9441	-25.4210	.1949	3.0081	554.9443	75.2823
683.5938	53.7456	.1000	-.9441	-25.4210	.2247	3.0081	647.4350	75.5391
781.2500	56.8538	.1000	-.9441	-25.4210	.2569	3.0102	739.9257	78.6774
878.9062	59.1404	.1000	-.9441	-25.4210	.2921	3.0104	832.4164	80.9990
976.5625	58.9211	.1000	-.9441	-25.4210	.3306	3.0103	924.9071	80.8183
1074.2188	59.3738	.1000	-.9441	-25.4210	.3724	3.0103	1017.3978	81.3128
1171.8750	58.6796	.1000	-.9441	-25.4210	.4178	3.0103	1109.8885	80.6640
1269.5313	58.3677	.1000	-.9441	-25.4210	.4668	3.0103	1202.3792	80.4012
1367.1875	59.1110	.1000	-.9441	-25.4210	.5195	3.0103	1294.8700	81.1971
1464.8438	58.3366	.1000	-.9441	-25.4210	.5758	3.0103	1387.3607	80.4791
1562.5000	57.8131	.1000	-.9441	-25.4210	.6354	3.0103	1479.8514	80.0155
1660.1563	57.5196	.1000	-.9441	-25.4210	.6995	3.0103	1572.3421	79.7857
1757.8125	57.6135	.1000	-.9441	-25.4210	.7669	3.0103	1664.8328	79.9470
1855.4688	57.2093	.3000	-.9441	-25.4210	.8379	3.0103	1757.3235	79.8139
1953.1250	56.4097	.5000	-.9441	-25.4210	.9126	3.0103	1849.8142	79.2889
2050.7813	54.3347	.5000	-.9441	-25.4210	.9910	3.0103	1942.3049	77.2923
2148.4375	53.7986	.5000	-.9441	-25.4210	1.0730	3.0103	2034.7956	76.8382
2246.0938	54.3712	.5000	-.9441	-25.4210	1.1586	3.0103	2127.2863	77.4964
2343.7500	54.5292	.4000	-.9441	-25.4210	1.2479	3.0103	2219.7771	77.6436
2441.4063	53.6779	.2000	-.9441	-25.4210	1.3406	3.0103	2312.2678	76.6851
2539.0625	53.0521	.1000	-.9441	-25.4210	1.4369	3.0103	2404.7585	76.0556

TABLE IV.- Continued

CODE FOR CORRECTIONS MADE:  
 IC=INSTRUMENTATION  
 CA=CONVECTIVE AMPLIFICATION  
 IS=INVERSE SQUARE LAW  
 AA=ATMOSPHERIC ABSORPTION  
 GI=GROUND IMPEDANCE  
 DF=DOPPLER FREQUENCY SHIFT

FREQUENCY	AVG SPL,DB	DELTA SPL (IC)	DELTA SPL (CA)	DELTA SPL (IS)	DELTA SPL (AA)	DELTA SPL (GI)	FREQUENCY (DF)	AVG SPL,DB FINAL
2636.7188	52.2451	-.2000	-.9441	-25.4210	1.5368	3.0103	2497.2492	75.0485
2734.3750	50.4089	-.2000	-.9441	-25.4210	1.6402	3.0103	2589.7399	73.3157
2832.0313	49.3276	-.2000	-.9441	-25.4210	1.7470	3.0103	2682.2306	72.3412
2929.6875	50.7291	-.2000	-.9441	-25.4210	1.8573	3.0103	2774.7213	73.8530
3027.3438	50.6315	-.2000	-.9441	-25.4210	1.9711	3.0103	2867.2120	73.8692
3125.0000	50.1119	-.2000	-.9441	-25.4210	2.0882	3.0103	2959.7027	73.4668
3222.6563	49.5724	-.2000	-.9441	-25.4210	2.2067	3.0103	3052.1935	73.0477
3320.3125	49.0908	.1000	-.9441	-25.4210	2.3325	3.0103	3144.6842	72.9900
3417.9688	48.3656	.1000	-.9441	-25.4210	2.4597	3.0103	3237.1749	72.3919
3515.6250	48.4253	0.0000	-.9441	-25.4210	2.5901	3.0103	3329.6656	72.4821
3613.2813	47.3814	0.0000	-.9441	-25.4210	2.7238	3.0103	3422.1563	71.5717
3710.9375	46.4380	0.0000	-.9441	-25.4210	2.8606	3.0103	3514.6470	70.7652
3808.5938	46.3110	0.0000	-.9441	-25.4210	3.0007	3.0103	3607.1377	70.7784
3906.2500	46.3373	0.0000	-.9441	-25.4210	3.1439	3.0103	3699.6284	70.9479
4003.9063	46.3915	0.0000	-.9441	-25.4210	3.2902	3.0103	3792.1191	71.1483
4101.5625	49.2773	.3000	-.9441	-25.4210	3.4396	3.0103	3884.6099	74.4835
4199.2188	55.1440	.5000	-.9441	-25.4210	3.5923	3.0103	3977.1006	80.7026
4296.8750	51.4247	.5000	-.9441	-25.4210	3.7474	3.0103	4069.5913	77.1387
4394.5313	44.8780	.5000	-.9441	-25.4210	3.9058	3.0103	4162.0820	70.7504
4492.1875	44.5357	.4000	-.9441	-25.4210	4.0671	3.0103	4254.5727	70.4695
4589.8438	43.7627	.4000	-.9441	-25.4210	4.2313	3.0103	4347.0634	69.8607
4687.5000	43.4372	.4000	-.9441	-25.4210	4.3984	3.0103	4439.5541	69.7022
4785.1563	43.1487	.4000	-.9441	-25.4210	4.5682	3.0103	4532.0448	69.5835
4882.8125	42.9284	.3000	-.9441	-25.4210	4.7409	3.0103	4624.5355	69.4358
4980.4688	42.7739	.4000	-.9441	-25.4210	4.9162	3.0103	4717.0262	69.5568
5078.1250	41.9997	.4000	-.9441	-25.4210	5.0943	3.0103	4809.5170	68.9606
5175.7813	41.1416	.4000	-.9441	-25.4210	5.2750	3.0103	4902.0077	68.2832
5273.4375	41.1212	.4000	-.9441	-25.4210	5.4584	3.0103	4994.4984	68.4462
5371.0938	40.8899	.4000	-.9441	-25.4210	5.6443	3.0103	5086.9891	68.4008
5468.7500	40.6599	.4000	-.9441	-25.4210	5.8327	3.0103	5179.4798	68.3592
5566.4063	40.9402	.4000	-.9441	-25.4210	6.0237	3.0103	5271.9705	68.8305
5664.0625	39.6241	.4000	-.9441	-25.4210	6.2171	3.0103	5364.4612	67.7078
5761.7188	39.1763	.4000	-.9441	-25.4210	6.4129	3.0103	5456.9519	67.4558
5859.3750	39.0159	.4000	-.9441	-25.4210	6.6110	3.0103	5549.4426	67.4935
5957.0313	39.2837	.4000	-.9441	-25.4210	6.8115	3.0103	5641.9334	67.9618
6054.6875	38.8418	.4000	-.9441	-25.4210	7.0143	3.0103	5734.4241	67.7228
6152.3438	38.6362	.3000	-.9441	-25.4210	7.2193	3.0103	5826.9148	67.6222
6250.0000	39.0901	0.0000	-.9441	-25.4210	7.4266	3.0103	5919.4055	67.9833
6347.6563	38.1248	-.2000	-.9441	-25.4210	7.6363	3.0103	6011.8962	67.0274
6445.3125	37.2942	-.2000	-.9441	-25.4210	7.8475	3.0103	6104.3869	66.4082
6542.9688	37.3899	-.3000	-.9441	-25.4210	8.0610	3.0103	6196.8776	66.6175
6640.6250	36.1088	-.3000	-.9441	-25.4210	8.2767	3.0103	6289.3683	65.5521
6738.2813	35.2681	-.3000	-.9441	-25.4210	8.4943	3.0103	6381.8590	64.9290
6835.9375	34.6389	-.3000	-.9441	-25.4210	8.7138	3.0103	6474.3498	64.5194
6933.5938	34.9896	-.4000	-.9441	-25.4210	8.9353	3.0103	6566.8405	64.9915
7031.2500	35.4036	-.5000	-.9441	-25.4210	9.1586	3.0103	6659.3312	65.5289
7128.9063	33.8830	-.5000	-.9441	-25.4210	9.3838	3.0103	6751.8219	64.2334
7226.5625	34.7338	-.5000	-.9441	-25.4210	9.6107	3.0103	6844.3126	65.3111
7324.2188	34.0523	-.5000	-.9441	-25.4210	9.8394	3.0103	6936.8033	64.8584

TABLE IV.- Concluded

CODE FOR CORRECTIONS MADE:  
 IC=INSTRUMENTATION  
 CA=CONVECTIVE AMPLIFICATION  
 IS=INVERSE SQUARE LAW  
 AA=ATMOSPHERIC ABSORPTION  
 GI=GROUND IMPEDANCE  
 DF=DOPPLER FREQUENCY SHIFT

FREQUENCY	AVG SPL,DB	DELTA SPL (IC)	DELTA SPL (CA)	DELTA SPL (IS)	DELTA SPL (AA)	DELTA SPL (GI)	FREQUENCY (DF)	AVG SPL,DB FINAL
7421.8750	32.7365	-.5000	-0.9441	-25.4210	10.0698	3.0103	7029.2940	63.7729
7519.5313	32.2565	-.5000	-.9441	-25.4210	10.3019	3.0103	7121.7847	63.5250
7617.1875	33.2204	-.5000	-.9441	-25.4210	10.5355	3.0103	7214.2754	64.7226
7714.8438	32.1509	-.5000	-.9441	-25.4210	10.7708	3.0103	7306.7661	63.8883
7812.5000	32.1942	-.2000	-.9441	-25.4210	11.0076	3.0103	7399.2569	64.4684
7910.1563	32.1595	.0000	-.9441	-25.4210	11.2458	3.0103	7491.7476	64.8720
8007.8125	30.7773	0.0000	-.9441	-25.4210	11.4855	3.0103	7584.2383	63.7295
8105.4687	31.8104	0.0000	-.9441	-25.4210	11.7267	3.0103	7676.7290	65.0038
8203.1250	31.5509	0.0000	-.9441	-25.4210	11.9693	3.0103	7769.2197	64.9867
8300.7812	31.3740	.3000	-.9441	-25.4210	12.2131	3.0103	7861.7104	65.3537
8398.4375	31.9610	.3000	-.9441	-25.4210	12.4583	3.0103	7954.2011	66.1859
8496.0937	31.3971	.1000	-.9441	-25.4210	12.7048	3.0103	8046.6918	65.6684
8593.7500	31.4105	.1000	-.9441	-25.4210	12.9524	3.0103	8139.1825	65.9295
8691.4062	33.4376	.1000	-.9441	-25.4210	13.2012	3.0103	8231.6733	68.2054
8789.0625	34.1192	.1000	-.9441	-25.4210	13.4512	3.0103	8324.1640	69.1371
8886.7187	35.2292	.1000	-.9441	-25.4210	13.7023	3.0103	8416.6547	70.4982
8984.3750	31.8769	0.0000	-.9441	-25.4210	13.9545	3.0103	8509.1454	67.2980
9082.0312	32.1857	0.0000	-.9441	-25.4210	14.2077	3.0103	8601.6361	67.8600
9179.6875	31.6757	0.0000	-.9441	-25.4210	14.4619	3.0103	8694.1268	67.6042
9277.3437	29.4498	0.0000	-.9441	-25.4210	14.7171	3.0103	8786.6175	65.6335
9375.0000	29.0355	0.0000	-.9441	-25.4210	14.9731	3.0103	8879.1082	65.4752
9472.6562	29.5821	0.0000	-.9441	-25.4210	15.2301	3.0103	8971.5989	66.2789
9570.3125	32.3836	0.0000	-.9441	-25.4210	15.4880	3.0103	9064.0897	69.3382
9667.9687	33.8459	.1000	-.9441	-25.4210	15.7466	3.0103	9156.5804	71.1591
9765.6250	33.4964	.2000	-.9441	-25.4210	16.0061	3.0103	9249.0711	71.1691
9863.2812	35.6565	.2000	-.9441	-25.4210	16.2663	3.0103	9341.5618	73.5893
9960.9375	36.2380	.2000	-.9441	-25.4210	16.5272	3.0103	9434.0525	74.4318

1. Report No. NASA TP-1898	2. Government Accession No.	3. Recipient's Catalog No.	
4. Title and Subtitle FLIGHT TEST OF A PURE-TONE ACOUSTIC SOURCE		5. Report Date October 1981	
		6. Performing Organization Code 505-32-03-04	
7. Author(s) Arnold W. Mueller and John S. Preisser		8. Performing Organization Report No. L-14600	
		10. Work Unit No.	
9. Performing Organization Name and Address NASA Langley Research Center Hampton, VA 23665		11. Contract or Grant No.	
		13. Type of Report and Period Covered Technical Paper	
12. Sponsoring Agency Name and Address National Aeronautics and Space Administration Washington, DC 20546		14. Sponsoring Agency Code	
		15. Supplementary Notes	
16. Abstract  A unique experiment involving static and flight testing of a pure-tone acoustic source has been conducted. The objectives of the experiment were (1) to determine if a 4-kHz tone radiated by a source in flight and mixed with broadband aircraft flyover noise could be measured on the ground with a high degree of statistical confidence, (2) to determine how well a comparison could be made of a flight-to-static tone radiation pattern and a static radiation pattern, and (3) to determine if there were any installation effects on the radiation pattern due to the flight vehicle. Narrow-band acoustic data were measured and averaged over eight microphones to obtain a high statistical confidence. The flight data were adjusted to an equivalent static condition by applying corrections for retarded time, spherical spreading, atmospheric absorption, ground impedance, instrumentation constraints, convective amplification, and the Doppler shift. The flight-to-static results are in excellent agreement with the measured static data. No installation effects were observed on the radiation pattern.			
17. Key Words (Suggested by Author(s)) Sound propagation Flight-to-static noise corrections Aircraft flyover noise		18. Distribution Statement Unclassified - Unlimited  Subject Category 71	
19. Security Classif. (of this report) Unclassified	20. Security Classif. (of this page) Unclassified	21. No of Pages 38	22. Price A03



National Aeronautics and  
Space Administration

Washington, D.C.  
20546

Official Business  
Penalty for Private Use, \$300

THIRD-CLASS BULK RATE

Postage and Fees Paid  
National Aeronautics and  
Space Administration  
NASA-451



3 1 10, H, 100681 500903DS  
DEPT OF THE AIR FORCE  
AF WEAPONS LABORATORY  
ATTN: TECHNICAL LIBRARY (SUL)  
KIRTLAND AFB NM 87117

**NASA**

POSTMASTER: If Undeliverable (Section 158  
Postal Manual) Do Not Return

---